Interannual Variability in an Indian Ocean Basin Model*

Johannes Loschnigg†
International Pacific Research Center‡
School of Ocean and Earth Science and Technology
University of Hawaii at Manoa, Honolulu, HI.

and

Peter J. Webster
Program in Atmospheric and Oceanic Sciences
University of Colorado at Boulder, Boulder, CO.

August 13, 2001

*SOEST contribution number xxxx and IPRC contribution number yy.

†*Corresponding author address:* Johannes Loschnigg, IPRC/SOEST, University of Hawaii at Manoa, 2525 Correa Road, Honolulu, HI 96822, USA. E-mail: johannes@soest.hawaii.edu

‡International Pacific Research Center is partly sponsored by Frontier Research System for Global Change.

Abstract

The behavior of the North Indian Ocean is examined using an intermediate ocean model forced by satellite and numerical model reanalysis data for the period 1984-1990. It is shown that there is substantial interannual variability in ocean dynamical and thermodynamical structures, commensurate with the atmospheric forcing. The heat balance for this region, particularly the meridional heat transport, undergoes strong variations related to the interannual variability of the monsoon. The magnitudes of the equatorial wave dynamics present in the Indian Ocean also show variations on interannual timescales. The relationship between the observed variability and the strength and characteristics of the Asian monsoon is explained in the context of sea-surface temperature (SST) - monsoon connections in the Indian Ocean. In particular, two of the years analyzed (1987 and 1988) illustrate the large differences in the strength of the ocean meridional circulation cell that is a key element in the cross-equatorial heat transports. It is hypothesized that the meridional heat transport may be an integral part of a coupled ocean-atmosphere system for this region, and that it may be considered as a process (among others) that can influence the interannual variability of the Asian monsoon.

1. Introduction

In response to the seasonal reversals of the annual monsoon winds, the tropical Indian Ocean undergoes large circulation transitions and strong annual and semi-annual variations in SST. In addition, coupled air-sea interactions combine to produce strong intraseasonal and interannual variability in circulations and rainfall of the south Asian summer monsoon. These variations are an important influence on a substantial percentage of the world's population who reside around the Indian Ocean rim. Accurate prediction of the interannual variability of the monsoon rains, as well as the intraseasonal variability, including severe weather such as tropical depressions and typhoons, is a critical concern for countries in this region.

Understanding the ocean processes in the tropical Indian Ocean may be a vital key in determining large-scale climate variability. The tight coupling of the tropical ocean and atmosphere has large climatic effects on a global scale (e.g., Palmer and Mansfield 1984; Webster and Lukas 1992; Webster 1994). Water vapor flux from the ocean is the primary source of monsoon rainfall, and the related latent heat release in the atmosphere and the perturbed radiational heating gradient drive planetary-scale atmospheric motions. Changes in the wind fields associated with the monsoon then force ocean currents which, in turn, modify the SST fields.

There is much debate as to whether interannual variability of SST in the tropical Indian Ocean is a key feature in the cycle of large-scale climate variability. Connections between the strength of the monsoon and the phase of the El Niño-Southern Oscillation (ENSO) phenomenon have been closely examined (e.g., Webster and Yang 1992; Joseph *et al.* 1994), showing that the influence of the monsoon is global in scale. Several studies (e.g., Rasmusson and Carpenter 1983; Mooley and Parthasarathy 1984) have shown that in general during recent decades, El Niño years are associated

with years of low All-India Rainfall Index (AIRI, following Parthasarathy *et al.* 1992) values and La Niña with high values, although the relationship between ENSO and the Asian monsoon appears to be weakening in recent decades (Krishna Kumar *et al.* 1999). Two years are of special interest for this study: 1987 was a strong El Niño year, followed by an equally strong La Niña in 1988. The two years correspond to weak and strong monsoon years, respectively, and are very different in terms of their atmospheric and oceanic signature (Krishnamurti *et al.* 1989; Krishnamurti *et al.* 1990). It is interesting to note that for the Indian Ocean region, the El Niño events of the protracted 1992-95 episodes and the unusually strong 1997-98 episode did not correspond to the canonical model of expected climate impacts from ENSO. Along with the possible weakening of the ENSO-monsoon relationship, the dynamics inherent to the Indian Ocean during 1997-98 created climate anomalies during this period that were different than those typically associated with El Niño conditions (Webster *et al.* 1999; Saji *et al.* 1999a). There have been a number of different types of ENSO events with protracted episodes similar to that of 1992-95 which would weaken the large scale ENSO-Indian Monsoon connections (Allan and D'Arrigo 1999; Reason *et al.* 2000).

Godfrey *et al.* (1995) noted that although the large variations in the Pacific Ocean SST field are considerably more important than those in the Indian Ocean for controlling ENSO events (Palmer *et al.* 1992), further progress in understanding ENSO may depend on deciphering the more subtle variations in the Indian and Atlantic Oceans. In analyzing the predictability of the monsoon in relation to both Pacific and Indian Ocean SSTs, Webster *et al.* (1998) suggest that the Indian Ocean SST appears to have less effect than SST anomalies in the Pacific Ocean in perturbing the the macroscale structure of the tropical climate, but that Indian Ocean SST anomalies may play a role in the "fine structure" of the monsoon such as the timing of the onset or the frequency and occur-

rence of monsoon active and break periods. However, the Godfrey *et al.* (1995) and Palmer *et al.* (1992) studies were based upon monsoon-ENSO interactions occurring in the 1980's. On longer timescales, Webster *et al.* (1998), Torrence and Webster (1998) and Torrence and Webster (1999) raise the possibility that variations in Indian Ocean SST may have a larger impact on the tropical climate during decades when ENSO variance is small. Several recent diagnostic studies have also suggested that SST distribution in the Indian Ocean is important in determining the strength of the monsoon. Warm Indian Ocean SST anomalies have been found to be a precursory signal to strong monsoon (e.g. Hastenrath 1987; Harzallah and Sadourny 1997; Sadhuram 1997; Meehl 1997; Clark *et al.* 2000), but signals of warming are only on the order of 0.5°C in observational studies.

Commenting on the modeling and prediction of tropical climate, Godfrey *et al.* (1995) note that nearly all of the skill demonstrated in current coupled models in forecasting a season or more in advance is due to improvements in modeling the global atmosphere or the dynamics and thermodynamics of the Pacific Ocean. Furthermore, models of the Indian Ocean are much less advanced. Compared to the similar atmospheric processes, heat storage and transport properties of the ocean are much more dependent on topographic detail, shown to be important in the Indian Ocean in a number of studies (Hsiung *et al.* 1989; Hastenrath and Greischar 1993; Wacongne and Pacanowski 1996; Garternicht and Schott 1997; Loschnigg and Webster 2000). Thus, the Indian Ocean may behave very differently in the manner in which it interacts with the climate system than do the other two oceans. Beyond acknowledging that unique phenomena exist in the Indian Ocean, Godfrey *et al.* (1995) note that details are not well understood at all. The aim of this study is to help understand the basic processes involved in the heat transport and how they combine to balance the heat budget of the North Indian Ocean.

Several studies have explored the annual mean and the seasonal cycle of the Indian Ocean

heat balance. The observational study of Levitus (1987) derived Ekman heat transport from the observed wind fields, while Hastenrath and Greischar (1993) and Hsiung *et al.* (1989) used climatological observational data and bulk formulas. The modeling studies of Garternicht and Schott (1997) and Wacongne and Pacanowski (1996) used an ocean GCM and the GFDL basin model, respectively, while Lee and Marotzke (1997) fit the dynamics of a general circulation model to climatological annual mean fields. Loschnigg and Webster (2000) use the $2\frac{1}{2}$ layer model of McCreary *et al.* (1993), forced by a climatological annual cycle of winds and surface fluxes. A brief overview of the annual cycle of heat transport will be given in section 2.

One component of the interannual variability of the Indian Ocean region is the tropospheric biennial oscillation (TBO, Yasunari 1991; Meehl 1987; Meehl 1993; Chang and Li 2000). This cycle is characterized by a "strong" monsoon year, with lower surface pressure over the northern Indian Ocean, higher northern Indian Ocean SSTs, and greater precipitation, convection and upward motion over the Indian region during the northern summer. A complex set of ocean-atmosphere interactions has been proposed by Meehl (1997) which progress into the western Pacific during the boreal winter season and is then followed by a "weak" monsoon year, in which the sub-tropical high in the Indian Ocean is substantially weakened, and higher pressure exists in the tropical Indian Ocean region along with cooler SSTs. Relatively less rainfall then occurs in the Indian summer monsoon, which is associated with weakened mean circulation. One of the problems with the processes proposed for the biennial oscillation is the maintenance of SSTs from one year to the next. Webster *et al.* (1999) have proposed a dynamical ocean-atmosphere process that forms a bridge between the extreme years of SST variability. In this study, we examine the possibility that the meridional heat transport on the Indian Ocean may also be an active component of interannual variations of climate in this region.

Nicholls (1989) also finds a pattern of correlation of Australian monsoon rainfall and the gradient of SST in the Indian Ocean that may be related to interannual variability of the cloud bands that emerge out of the eastern equatorial Indian Ocean and cross the Australian continent from the northwest to the southeast. Fasullo and Webster (1999) find these bands also extend north and eastward and are associated with intraseasonal variations of the SST in the eastern Indian Ocean. The effect studied in Nicholls (1989) suggests a change in the atmospheric circulation over the Indian Ocean basin on timescales corresponding to the interannual variability discussed previously. Nicholls (1989) concludes that events in the Indian Ocean have an important influence on Australian winter rainfall (and, according to Fasullo and Webster (1999), in south and south-east Asia), and that the existence of this relationship with the SST patterns observed are not closely associated with the Southern Oscillation. Nicholls' correlations account for some 40% of the variance of precipitation in southeast Australia.

Previous observational and modeling studies have shown the existence of equatorial waves in the Indian Ocean, which have effects on the currents, SST and the mixed layer. In this region, equatorial wave dynamics in the 26-day period range (of the mixed Rossby-gravity, or Yanai wave type), with variations in meridional velocity in the upper 200m have been observed by Luyten and Roemmich (1982), Reverdin and Luyten (1986), Tsai *et al.* (1992) and Reppin *et al.* (1999). The period of the waves observed by Reppin *et al.* (1999) were in the 15 day range - shorter period than that of previous studies. Modeling studies (Kindle and Thompson 1989; Woodberry *et al.* 1989; Moore and McCreary 1990; Jensen 1993) have simulated similar high-frequency dynamics. Various theories have been suggested as to the cause of such waves, among them the existence of a barotropic instability generated by the lateral shear between the south equatorial current and the north equatorial counter-current within the southern gyre, instabilities related to the

Somali current, and local wind forcing. Observational studies also suggest the existence of long-period wave dynamics in the equatorial Indian Ocean. Luyten and Roemmich (1982) deduced a mixture of an equatorial Kelvin wave and a long equatorial Rossby wave of the first meridional mode, with zonal wavelengths of 24,000 and 8000 km, respectively. The observed variations in zonal velocity in their study correspond to a period of 180 days. Jensen (1993) suggests that resonant wind-stress forcing can explain a strong semi-annual response. He argues that the basin geometry allows for resonant forcing of the second baroclinic mode, with an excitation of equatorial Kelvin (Rossby) waves which traverse the Indian Ocean in 1.5 (4.5) months, reflect at the eastern (western) boundary and transfer their energy to a westward (eastward) Rossby (Kelvin) wave. Similar wave dynamics in both the 26-day and 180-day periods are present in the McCreary *et al.* (1993) model, but this study illustrates year-to-year variations in wave activity that may result from changes in surface forcing.

In this study we analyze the variation of the upper ocean dynamics, specifically the heat balance and the wave dynamics, on interannual timescales, in order to examine their influence in determining the SST in the Indian Ocean. The response of the Indian Ocean to atmospheric forcing will be explored using an intermediate ocean model (McCreary *et al.* 1993) integrated over a number of years. This extended integration will allow the study of the adjustment of the ocean basin to widely varying surface meteorological conditions. The annual cycle of the Indian Ocean heat balance will be discussed in section 2. The data and model used are discussed in section 3. Section 4 begins with an analysis of interannual variability of SST and its relationship to large-scale monsoon variability. It continues with a discussion of the variation of the oceanic heat balance on interannual timescales, as well as the variability of the wave dynamics. Discussions and conclusions are presented in Section 5.

2. Annual Cycle of the Indian Ocean Heat Balance

The Indian Ocean has been shown to undergo a strong seasonal reversal in the both heat transport and storage (Loschnigg and Webster 2000). Peak magnitudes of heat transport ($\pm$ 2 PW) have been found to be substantially larger than the peak magnitudes of net surface heat flux (0.5 PW) over the annual cycle, especially in the northern regions. This large redistribution of heat through oceanic processes may be a key factor in effecting an interannual variability of climate in the Indian Ocean. The heat balance of the Indian Ocean has been explored on both the annual mean as well as the seasonal cycle, and early observational estimates of the Indian Ocean heat balance were able to capture the general magnitudes of the heat transport, as well as seasonal reversals (Levitus 1987; Hsiung *et al.* 1989; Hastenrath and Greischar 1993). Recent modeling efforts have gone further to describe the finer details of the heat transport and the underlying dynamics, as well as some of the interannual variability (Wacongne and Pacanowski 1996; Garternicht and Schott 1997; Lee and Marotzke 1997; Loschnigg and Webster 2000).

Wacongne and Pacanowski (1996) examined the seasonal reversal of heat transport in a multiple-layer Indian Ocean model which included analysis of deep ocean currents. Their results show an annual mean southward meridional heat transport at the equator of about -0.2 PW (1 PW = 10^{15}W, with negative transport denoting net southward heat transport), which agree qualitatively with observational studies (Hastenrath and Greischar 1993; Hsiung *et al.* 1989). Their maximum annual mean meridional heat transport is -0.55 PW at 13°S. They find cross-equatorial heat transports of -1.2 PW and +1.0 PW during the summer and winter seasons, respectively . Similar results were found by Garternicht and Schott (1997) using a global eddy-resolving model, who calculate an annual mean cross-equatorial heat transport to be -0.18 PW, and a maximum of -1.14 PW at

15°S. By fitting the dynamics of a general circulation model to climatological annual mean fields, Lee and Marotzke (1997) find an annual mean cross-equatorial heat transport of -0.4 PW, with a maximum of -0.9 PW at 15°S. Loschnigg and Webster (2000) also evaluated the annual cycle of cross-equatorial heat transport in the intermediate ocean model of McCreary *et al.* (1993), and its role in limiting the SST increases in a region of strong net surface heat flux into the ocean. Loschnigg and Webster (2000) also found seasonal mean cross-equatorial heat transports of -1.5 PW and +1.0 PW during the northern summer and winter seasons, respectively, and an annual mean of -0.13 PW, in agreement with other modeling studies. In their study, it was found that peak magnitudes of heat transport ($\pm$ 2 PW) were substantially larger than the peak magnitudes of net surface heat flux (0.5 PW) over the annual cycle, especially in the northern regions. They showed that on seasonal timescales, the heat balance of the northern Indian Ocean is basically dominated by a balance between heat storage in the upper ocean layers and cross-equatorial meridional heat advection. Much of the seasonal reversal of the monsoonal wind stresses is a key factor in developing the annual cycle of meridional heat transport. These findings are similar to those of Wacongne and Pacanowski (1996) and Garternicht and Schott (1997), where the basic features of heat transport in the Indian Ocean are a northward boundary current of cool water, upwelled in near the coasts of Somalia and Oman, and returned southward through interior surface currents at warmer temperatures. Ekman transport is found to be a large factor in reversing the direction of the net heat transport, but Wacongne and Pacanowski (1996) find that deeper layers must also be involved in the process, including seasonal changes in the deep western boundary current. This large redistribution of heat through oceanic processes may be a key factor in effecting an interannual variability of climate in the Indian Ocean.

Figure 1a shows a comparison of the annual mean heat transport from various observational

and modeling studies listed above (note that the results for Levitus (1987) are for the wind driven Ekman transports only). Results from the Loschnigg and Webster (2000), show generally good agreement with the previously mentioned studies. The major differences are a slightly larger mean southward transport at 5°S, and slightly weaker southward (and even some northward) mean transport in the areas near 20°S. Figure Figure 1b (adapted from Loschnigg and Webster 2000) shows a schematic of the basic seasonal cycle of the heat balance of the North Indian Ocean as simulated in a $2\frac{1}{2}$ layer ocean model. Net surface heating in the North Indian Ocean in boreal spring and summer is balanced by strong southward magnitudes of hear transport in the boreal spring and summer months, along with decreases in heat storage. In boreal winter, the revere situation occurs, with net surface heat loss in the North Indian Ocean balanced by northward heat transport and increases in heat storage. The reversal of the values of heat transport between summer and winter may be thought of as a seasonally reversing meridional circulation cell, as described by McCreary *et al.* (1993) and Wacongne and Pacanowski (1996). Previous studies have focused generally on the mechanisms and dynamics of the tropical Indian Ocean heat balance and its relationship to surface heat flux and heat storage for a mean annual cycle. Loschnigg and Webster (2000) emphasized the seasonal variation of the heat balance. The recent studies of Murtugudde and Busalacci (1999) and Behera *et al.* (2000) simulate interannual SST variability, and examine how the surface heat fluxes influence SST anomalies. In this paper, we will investigate how the heat balance of the Indian Ocean varies on interannual timescales, and how this variability may interact with the Indian monsoon.

3. Data and Model

The multi-year integrations were performed using data from the NCEP-NCAR reanalysis data set (Kalnay *et al.* 1996) for the period 1984-1990 for surface winds, air temperature and specific humidity. Although some aspects of the NCEP reanalysis data has been shown to have minor disagreements with observations over the Indian Ocean - Asian Monsoon region, the basic features of the monsoon surface circulation are well reproduced (Annamalai *et al.* 1999). For the surface radiational flux forcing, we utilize surface net solar shortwave (SW) radiation flux data from the Bishop and Rossow (1991) dataset derived from the cloud retrievals from the International Satellite Cloud Climatology Project (ISCCP) data, and available daily for the period July 1983 - June 1991. Net surface longwave (LW) radiation fluxes are obtained from the ISCCP derived surface radiation budget (SRB) dataset (Darnell *et al.* 1992), which provides fluxes on a monthly averaged basis. Observed SST fields used for comparison are obtained from Reynolds SST (Reynolds and Smith 1994). All data is averaged or interpolated to 5-day means for both analysis and model forcing.

The model used in this analysis is the same as described in Loschnigg and Webster (2000), where greater detail may be found. We use the $2\frac{1}{2}$ layer ocean model of McCreary *et al.* (1993), which has been shown to simulate successfully many of the circulation features of the upper Indian Ocean (McCreary *et al.* 1993; Loschnigg and Webster 2000), including the seasonally-reversing meridional circulation cell that appears to be important for the Indian Ocean heat transport. Since the annual cycle and basic features of the Indian Ocean are so well reproduced by a relatively simple $2\frac{1}{2}$ layer model, we choose this intermediate model over more complex multi-layer or ocean GCM models so as to simulate interannual variability in the upper ocean in a manner that is less

dynamically complex but yet reveals fluctuations in the heat balance on longer period time scales. Although the model has some flaws that limit its ability to replicate some of the finer features of the regional dynamics, the model is successful at simulating the large-scale currents involved in the redistribution of heat in the region (Han and McCreary 2001).

For this study, the model run is spun-up from a state of rest beginning on April 15, which climatologically is a weak wind period in the northern Indian Ocean. To inhibit the excitation of inertial oscillations, the wind stress driving the model is ramped up from zero to the observed level over a 5-day period. The model is integrated forward in time using forcing fields for the year 1984 as a continuous annual cycle for 7 model years at which time the model approaches a stable annual cycle. The forcing is then changed to successive fields corresponding to subsequent years. Results shown are for the years 1984-1990, the period for which daily SW data is available.

4. Results

4.1 Comparisons of model and observed upper ocean temperatures

Loschnigg and Webster (2000) showed that the McCreary *et al.* (1993) model was quite capable of replicating the climatological SST distribution in the Indian Ocean. Here we focus on the years 1987 and 1988, as these are years of particular interest for this study. Distribution of Reynolds SST and model mixed layer surface temperature (T_m) for the boreal summer monsoon months of June through August for 1987 and 1988 are shown in Fig. 2. Both observations and model show slightly warmer conditions for 1988 as compared to 1987. The model SST is slightly warmer than Reynolds in the Arabian Sea and the Bay of Bengal, while slightly cooler in the eastern equatorial regions. Discrepancies between observations and model surface temperature

may be due to factors such as the lack of salinity or a barrier layer in the model, as well as the lack of an Indonesian throughflow. When the observations and model surface temperatures are compared regionally (e.g. regions extending 10°in latitude and 20°in longitude) during the period 1984 - 1990, correlations of 0.8 or higher were found.

The model reproduces the interannual variability of observed upper ocean temperature anomalies in in the Indian Ocean. Figure 3 shows the T_m anomalies (with the annual and semi-annual cycles removed) of the northern and southern Indian Ocean regions. These timeseries show anomalous warming beginning in mid-1987 (concurrent with the weak Indian summer monsoon of 1987). The warming continues into 1988, shifting back to cool anomalies in late 1988 after the strong boreal summer monsoon of that year. Behera *et al.* (2000) also find warm SST anomalies for this period in their simulation. When a similar region-by-region analysis (as mentioned above) is performed for the SST anomalies, correlations for the regions are 0.4 or better.

Interannual variability in the ocean model is also evident in Hovmöller diagrams of the layer 1 meridional current velocity (v_1) for 1987 and 1988 shown in Fig. 4. The two years show a very different structure. Greater variance occurs during the strong monsoon year of 1988 than the weak monsoon year of 1987, presumably because of larger windspeeds during 1988. Figure 5 shows the difference between 1988 and 1987 windspeeds for June-August. It is evident that in 1988 there is greater mean windspeeds for June-August in the monsoon gyre, especially for the region of the central Indian Ocean basin between 10°S and 3°N, and for the northern Arabian Sea. Figure 6 shows a Hovmöller diagram of equatorial model layer 1 zonal currents (u_1) for 1984-1990. (The lines $A-A'$ and $B-B'$ in Fig. 6 will be described in section 4.3). More amplitude in zonal current variability is seen in late 1988 as compared to 1987 in the central and eastern part of the basin. We will discuss the interannual variability seen in these figures as they relate to both the heat transport

and the equatorial wave dynamics in sections 4.2 and 4.3.

4.2 Heat Balance

In the present analysis of the heat balance of this region, it is shown that the characteristics of the heat transport and heat storage of the northern Indian Ocean exhibit substantial interannual variability, and that the Indian Ocean has a remarkable ability to equilibrate in the presence of vastly differing atmospheric conditions. When the heat balance is viewed over a long time span as analyzed here, the influence of large-scale phenomenon such as an overall strong or weak monsoon year, as well as the phase of ENSO, affect the important parameters that drive the ocean dynamics and thermodynamics. The major components of the oceanic heat balance are heat transport, heat storage and surface heat flux. In this study, the method of calculating the heat balance for the model is equivalent to that in Loschnigg and Webster (2000).

Loschnigg and Webster (2000) have shown that the North Indian Ocean heat balance undergoes considerable interannual variability, particularly in the years 1987 and 1988, which are interesting as they represent, respectively, substantially weak and strong years of the south Asian monsoon, as well as the El Niño and La Niña phases of the ENSO cycle. They show that, for the annual mean, the southward heat transport is substantially reduced in 1987, and is accompanied by a large increase in heat storage, while an almost complete reversal of this situation occurs in 1988, with massive southward heat transport and a reduction of the net heat storage of the North Indian Ocean (Figure 12b of Loschnigg and Webster 2000). Figure 7 displays this situation, showing annually averaged total heat transport (Q_v) as a function of latitude for the years 1984-1990. North of about 10°S, 1988 shows the strongest southward heat transport, with values at 5°S being substantially greater than those of other years. In contrast, 1987 has the weakest southward heat transport

for latitudes north of about 7°S. In the presence of such strong interannual variability, the average North Indian Ocean SST does not change more than 0.5 - 1.0°C, making the Indian Ocean unique in its ability to come to a state of relative equilibrium while very large changes of external atmospheric forcing occurs. This relatively constant SST on interannual timescales is likely a consequence of the magnitude of the meridional heat transports.

To understand the dynamics behind this interannual variability, we undertake a similar analysis which Loschnigg and Webster (2000) carried out for the climatological annual cycle, and apply it to the specific years in question here. We break down the heat transport into two major components: the wind-driven Ekman component $Q_{v(EK)}$ and the geostrophic component $Q_{v(G)}$. The Ekman transports are calculated from the NCEP reanalysis derived surface wind stresses. The geostrophic component can then be derived as

$$Q_{v(G)} = Q_{v(TOT)} - Q_{v(EK)} \tag{1}$$

where $Q_{v(TOT)}$ is similar to the total heat transport Q_v, but for the interior ocean only (further than 3°longitude from any boundary) so as to allow for a proper comparison to the interior Ekman transport. The geostrophic flow results from meridional variations in layer depths and layer temperatures, which, collectively, generate density gradients and pressure forces (Loschnigg and Webster 2000).

Figure 8 shows the zonally integrated values for each of these components of the meridional heat transport ($Q_{v(EK)}$ and $Q_{v(G)}$) plotted as a function of latitude for the Indian Ocean for the climatological annual mean, Jun-Aug and Jan-Feb (based on a 1984-1990 climatology). As balances in the Ekman theory break down as one approaches the equator, values for $Q_{v(EK)}$ and $Q_{v(G)}$ are shown only for regions north of 4°N. Figure 8a shows that for the Indian Ocean north of

about 10°S, it is the Ekman, or the wind-driven component of the heat transport that is the major contributor of transport. South of 10°S, the geostrophic component provides a strong northward transport, balancing the southward Ekman component near 15°S. South of 15°S, the southward Ekman component weakens, and the geostrophic component remains strongly northward, producing net northward transport. The geostrophic component of the transport varies little over the annual cycle, remaining northward over most seasons at most latitudes (Figs. 8b and c). The seasonal variation of transport is accomplished through the seasonal reversal of the monsoon winds over the Indian Ocean. Figure 9 shows an analysis of the relationship between zonally integrated mean zonal wind and the heat transport at various latitudes over the climatological annual cycle. There is a strong correlation ($\geq$ 0.9 at latitudes north of 20°S) between the seasonal reversal of the surface zonal winds to the seasonal reversal of the heat transport, similar to the results of Garternicht and Schott (1997). While of significant strength at southern latitudes, the geostrophic component plays a much lesser role in the seasonal heat transport variations.

We now examine how the variation of the surface monsoon winds affect the interannual variability of the heat transport. Figure 10 shows the Ekman heat transport ($Q_{v(EK)}$) for the two extreme years of 1987, 1988 (the weak and strong monsoon years, respectively) and the 1984-1990 climatological mean. For the annual mean (Fig. 10a), the Ekman component in 1988 clearly shows stronger southward heat transport than average, especially in the peak region of 5°to 10°S. In the same latitudes, the values for 1987 are below average. In the northern regions (5°to 15°N), the results for 1988 are somewhat stronger than average, while those for 1987 are again below average. For the JJA mean (Fig. 10b), the larger Ekman component of 1988 over the other years in the areas of 5°to 10°S is clearly seen, while 1987 is slightly below average. Similar to the annual mean, 1988 dominates slightly over the climatology in the northern regions, while 1987 is slightly

weaker. For the winter months of Jan-Feb. (Fig. 10b), 1988 shows a much weaker than average northward Ekman component in the 5°to 10°S region, helping to bring the annual mean 1988 heat transport to strong southerly values. The values for 1987 are either near normal or, in the northern latitudes, somewhat stronger northward than the mean. It can also be noted that south of 10°S the Ekman component remains southward during all seasons, owing to the year-round easterlies at these southern latitudes. From Fig. 10, we can see how the strong interannual variability of the the meridional heat transport in the Indian Ocean (as shown in Loschnigg and Webster 2000) is primarily due to the variation in the Ekman transport, a principle component of the wind-driven circulation cell mentioned by McCreary *et al.* (1993). Variations in monsoon strength, and thus surface wind speed as seen in Fig. 5, are a primary factor in the large deviations from normal in the Indian Ocean heat balance. In section 5, we discuss how this process may interact with the monsoon to enhance a biennial cycle in the Indian Ocean region.

4.3 Equatorial Waves in the Indian Ocean

We now examine the wave structure of the Indian Ocean basin to determine their impact on the upper ocean currents, mixed layer depth and mixed layer temperature. Figure 11 shows a Power Hovmöller diagram (see Torrence and Compo 1998) of T_m and mixed layer depth (h_m) along the equator. A Power Hovmöller is an average of wavelet power between given periods for multiple points as a function of space. Wavelets are obtained from the time series of the T_m and h_m fields at discreet points along the equator. The resulting power of each wavelet is averaged over the 10 to 60 day period range to obtain a power versus time analysis for points along the equator. The period band is chosen to capture the high frequency dynamics in the model basin. Figure 11a shows a substantially increased short-period power in T_m during the summer of 1988.

This increased variance in 1988 is also seen in the h_m field (Fig. 11b) where it is substantially greater than the summer of 1987. The differences between the summers of 1987 and 1988 will be shown to be related to different strengths of equatorial wave activity, which is substantially greater in the simulation of 1988 than 1987. The differences between these two years in terms of monsoon strength, surface winds and oceanic response was noted earlier. We will focus on these two years for further analysis.

In the layer 1 meridional current velocity (v_1) Hovmöller diagrams for 1987 and 1988 shown in Fig. 4 earlier, it was noted that differences in the variance between these years was likely due to variations in the strength of the monsoon winds during the boreal summer season. Figures 12a and 12b show wavelet power spectra for equatorial v_1 and u_1 (respectively) in the eastern Indian Ocean (80°E). We first turn to the analysis of v_1, and will discuss u_1 below. Short period variability (10-25 days) is evident in v_1 (Fig. 12a) at certain parts of the year during the entire time analyzed. Most notably, the strongest variability occurs in mid- to late-summer, after the monsoon onset. This is likely due to the oceanic response from the accelerating monsoon winds. Larger variance in these short-period ranges is also evident during the springtime transition period between the winter and summer monsoon in some years, which suggests that the wave dynamics may be an oceanic response and relaxation between periods of strong wind stress. Figure 13a shows a Power Hovmöller of equatorial v_1 within the 10 to 60 day period range (the Power Hovmöller of equatorial u_1 in Fig. 13b will be discussed below). Although not quite as clear as Fig. 12a, it is evident that 1988 has relatively higher power in the 10 to 60 day period range during 1988 compared to 1987. In all 7 years, the general propagation of wave (group) energy is eastward, initiating every boreal summer during the onset of the south Asian monsoon (usually late May to early June). Boreal wintertime eastward propagation begins in January of each year, corresponding to the transition of

the wind field over the ocean basin to the Australian monsoon.

Fig. 14 shows the wavenumber-frequency spectrum dispersion relation for the equatorial meridional current field (v_1) over the 7 years. Peak power is centered around the $n = 0$ solution (curved solid line) for a westward propagating phase (eastward propagating group) equatorial Rossby-gravity (Yanai) wave with an equivalent depth of $H_e = 0.13m$ (Matsuno 1966). The variance seen in the central and western part of the model basin in both the 1987 and 1988 Hovmöller diagrams of Fig. 4 can thus be described as mixed Rossby-gravity waves with periods of about 16 to 17 days and wavenumbers of order -10 (the negative sign denoting a westward phase propagation), and an eastward group propagation. With the equivalent depth of $H_e = 0.13m$, shallow water theory predicts a propagation speed of $c = \sqrt{gH_e} = 1.13\ msec^{-1}$, which is similar to the characteristic speed of the second baroclinic mode of 1.25 $msec^{-1}$ as calculated by McCreary *et al.* (1993). Most of the power in Fig. 14 is located in the periods between 16 and 17 days, which is in agreement with the observations of Reppin *et al.* (1999), but slightly shorter than that of other studies. These wave dynamics are evident in Fig. 15, which shows the layer 1 current vectors for August 13th and 18th of the modeled year 1984. A propagation of alternating southward and northward meridional currents is seen traveling eastward across the basin at the equator, moving about 20°of longitude during the five days shown. The zero absolute vorticity line (thick solid line in Fig. 15) also shows some meridional deviation from the equator propagating westward.

Figure 16 shows the corresponding wavenumber-frequency dispersion relation for u_1 (relating to the Hovmöller diagram of Fig. 6). Power at 180 day periods is seen in a westward propagating mode, similar to that seen in the observational study of Luyten and Roemmich (1982). The two solid lines in Fig. 16 show the dispersion curves for the equatorial $n = 1$ Rossby wave (left side) and the equatorial $n = 1$ Kelvin wave (right side), both with an equivalent depth of $H_e = 0.13m$.

The westward propagating Rossby wave can be seen in Fig. 6 as the line $B - B'$. The shorter period eastward Kelvin wave is seen in Fig. 6 as the line $A - A'$.

Figure 12b shows a wavelet spectrum of model equatorial zonal velocity at 80°E. Substantial power is seen in the long periods, but most of the power resides in the 180-day period range. The boreal summers of 1987 and 1988 is a time when the power seen in the 180-day period range is strongest. Figure 13b shows the Power Hovmöller for equatorial u_1 for the period range of 100-250 days. The eastern Indian Ocean is the location for the dominant power of long period wave activity, with substantially greater power during the boreal summer of 1988 compared to that of other years. Note that during the years 1987 and 1988, the location of the minimum power changes more towards the western side of the basin, and then returns to the center once again in late 1989. During this period, and particularly in 1988, substantial power is seen in the eastern side of the basin.

5. Discussion and Conclusion

The variability of the surface fluxes, heat balance and dynamical structure of the upper Indian Ocean have been analyzed using an ocean model to investigate the response of the Indian Ocean to interannual variability of wind and thermal forcing. The model was forced with surface meteorological data for a seven year period. Strong interannual variability in the dynamics of the model layers is observed that has clear connections with the surface wind driven currents associated with the strength of the Asian summer monsoon.

Generally good agreement was found between model T_m and SST, in terms of anomalies from the annual cycle. Similarities between the two fields include the substantial basin-wide warming

during the boreal winter of 1987-1988, which has been shown to be a precursor to a strong monsoon cycle (Meehl 1997). Strong interannual variability of the surface meteorological conditions leads to substantial changes in the structure of the upper ocean. Wave activity has been shown to vary greatly between the years simulated. The wavelets and Power Hovmöllers show large variations in the locations and power of oscillations in the upper layer current fields associated with the variations in surface forcing conditions.

The process of meridional heat transport in the Indian Ocean is so important to this region that the SSTs of the North Indian Ocean remain relatively constant (varying by only 0.5 - 1.0°C) over long periods, while variations in the surface forcing conditions and upper ocean heat balance dynamics can change substantially. Loschnigg and Webster (2000) discuss the meridional heat transport in the Indian Ocean as part of a suite of processes which exist to regulate warm pool SST. In their study, they find that SST is regulated as a part of an overall adjustment of the system (not just at the surface through changes in radiative and latent heat fluxes), and relaxation occurs through a combination of thermodynamical feedbacks and atmospheric and oceanic transports of heat. In this region, unlike in the tropical western Pacific Ocean "warm pool", local thermodynamical processes or atmospheric processes are not of sufficient strength to regulate SST, due to local constraints such as the externally forced subsidence in the North Indian Ocean, and the upper ocean can only relax through oceanic processes. The large interannual variability of ocean dynamics seen in the simulation here, with upper ocean temperatures remaining within a fairly constant range, is an illustration of the Indian Ocean basin achieving balance through strong oceanic dynamic processes.

It was shown that the years 1987 and 1988 were very different in terms of the strength of the Ekman component of heat transport, with 1988 having much stronger southward transport than

average, and 1987 having a weaker than normal transport. It is possible that this strong variation of ocean dynamics may play a role in the biennial cycle of Indian-Pacific Ocean climate variability (Meehl 1987; Meehl 1993). In most of the theories to the TBO, anomalies of Indian Ocean SST play a significant role in the development of the biennial cycle, but they are generally considered in terms of anomalies of upper-ocean heat storage created by one-dimensional local interactions with the surface fluxes, and which exist over multiple seasons to link one monsoon season to the next (Yasunari 1991; Meehl 1993). As noted earlier, a number of studies have shown that Indian Ocean SST anomalies in the winter and spring correlate strongly with the strength of the following monsoon. Chang and Li (2000) allude to the role that the heat transport may play in the development of a biennial cycle in the Indian Ocean region, but they do not include this process in their simple model. Although the temporal length of this study is far too short to significantly analyze the existence of a biennial signal in the heat transport, the results raise the possibility that the interaction of the monsoon and the wind-driven heat transport may assist in the dynamics of a TBO, as the simulated variation of heat transport on interannual timescales would enhance, rather than hinder a biennial cycle.

Consider the following scenario depicted in Figure 17: In a given summer, the meridional heating gradient developed from the warm land and cool ocean regions drives a cross-equatorial monsoon wind gyre, shown as the black streamlines in Fig. 17. The oceanic Ekman transport, associated with the monsoon winds are displayed as yellow arrows with mass transports to the right of the wind direction in the northern hemisphere and to the left in the southern hemisphere. Because of the characteristics of the monsoon gyre (generally westward south of the equator and eastward to the north), the direction of the Ekman transport is to the south on both sides of the equator. Variations in monsoon strength may occur from the influence of a variety of regional and

remote factors, such as the phase of ENSO (Shukla and Paolino 1983), more or less persistent winter snowfall over Eurasia (Yasunari *et al.* 1991; Vernekar *et al.* 1995), SST anomalies in the Indian or Pacific Oceans, stochastic processes in the southern Indian Ocean (Rodwell 1998) or chaotic processes (Palmer 1994). Thus a strong monsoon may develop during one summer season (Fig. 17a). Stronger than normal surface wind stresses (thick black streamlines) drive an anomalously large magnitudes of southward Ekman heat transport (thick yellow arrows), greatly lowering the net heat content and leaving cool SST anomalies in the northern Indian Ocean and Arabian Sea after the monsoon season (Fig. 17b). Loschnigg and Webster (2000) show that oceanic heat advection primarily effect the SSTs in this region These SST anomalies are typical of the TBO pattern of Indian Ocean SSTs described by Meehl (1997), and are also related to the Indian Ocean "Dipole" pattern of Webster *et al.* (1999). The cool SST anomalies persist to the following boreal springtime, and then assist in the development of a weak monsoon the following summer (Fig. 17c). Weaker than normal wind stresses (thin black streamlines) then result in lower than normal Ekman heat transport (thin yellow arrows), reducing the amount of heat content loss and leaving warm SST anomalies in the northern Indian Ocean and the Arabian Sea (Fig. 17d). The warm SST anomalies persist through the following springtime and assist in the development of a strong monsoon the following summer (Fig. 17a). This process may be thought of as an extension of the annual cycle of SST modulation in the Indian Ocean proposed by Loschnigg and Webster (2000). This cycle could be thus one of many processes that exist to affect the monsoon variation (along with Indian Ocean SST anomalies, Central and East Pacific SST anomalies, heating and atmospheric circulation anomalies over central and south Asia, and other previously mentioned factors). Meehl and Arblaster (2001) have attempted to show how these various processes may each have differing influences on the monsoon during different years. It is possible that the heat

transport (and resulting Indian Ocean SST anomalies) may be another factor to consider when examining interannual variability in monsoon rainfall.

Analysis of Asian monsoon and Indian Ocean process in the 300-year baseline run of the fully coupled NCAR Climate System Model (CSM) is currently under investigation. Preliminary results show that there is a reasonably high level of correlation between the Indian boreal summer monsoon and the cross-equatorial meridional oceanic heat transports. When the monsoon is measured as an index of the westerly wind shear (the 850mb minus 200mb U-shear for JJAS in the region 35°E to 75°E and 5°N to 15°N), the seasonal correlation of this index with the JJAS oceanic heat transport across the equator is -0.56 (the negative sign denoting stronger negative - southward - heat transports in JJAS with a stronger monsoon circulation). The JJAS heat transport is also correlated to the boreal fall Indian Ocean zonal SST anomaly gradient (Webster *et al.* 1999; Saji *et al.* 1999b). When measured as the difference in the SST anomalies between the western North Indian Ocean (the oceanic region within 0°S to 15°N and 45°E to 70°E) and the eastern equatorial Indian Ocean (10°S to 5°N and 85°E to 100°E), the Indian Ocean SST zonal mode correlates to the JJAS meridional heat transport at 0.42, showing the the boreal summer meridional heat transports are also related to the development of SST anomaly fields that may persist and develop anomalies in monsoon strength the following boreal summer season. (The correlations between the heat transport and the western North Indian Ocean region alone are 0.40. All correlations are significant at the 95% level.) This suggests that the ocean-atmosphere processes suggested here exist in coupled simulations to modulate the Asian monsoon and contribute to interannual variability. The full results of this coupled simulation will appear in a future paper.

Finally, it should be noted that there appear to be strong connections of phenomena across broad frequency domains. For example, following the studies of Palmer (1993), Palmer (1994), and

Ferranti *et al.* (1997), Webster *et al.* (1998) noted the similarity of intraseasonal and interannual principle patterns, and used this observation to suggest that the two scales were intimately linked. In fact, very strong intraseasonal variability appears within Indian Ocean heat transports which are strongly linked to atmospheric forcing (Loschnigg and Webster 2000). The intraseasonal variability of the Indian Ocean will be the subject of another paper.

Acknowledgments

This work has been supported by the Climate Dynamics and Large-scale Meteorology Divisions of the National Science Foundation under grant ATM-9526030, and by NASA under grant NAG 5-7485. Thanks to J. Curry, S. Godfrey and J. McCreary for helpful comments and suggestions during the course of this research. Thanks also to C. Torrence, G. Compo, D. Lawrence and M. Wheeler for assistance with analysis and graphics. Datasets were kindly provided by the following institutions: J. Bishop at Univ. of Victoria (for satellite derived net surface SW data), NASA (for satellite derived net surface LW data), NCAR (for Reanalysis data) and NOAA/CDC (for Reynolds SST data).

References

Allan, R.J., and R.D. D'Arrigo, 1999: 'Persistent' ENSO sequences: How unusual was the 1990-95 El Nino? *Holocene*, **9**, 101–118.

Annamalai, H., J. Slingo, K.R. Sperber, and K. Hodges, 1999: The Mean Evolution and Variability of the Asian Summer Monsoon: Comparison of ECMWF and NCEP-NCAR Reanalyses. *Mon. Wea. Rev.*, **127**, 1157–1186.

Behera, S.K., P.S. Salvekar, and T. Yamagata, 2000: Simulation of Interannual SST Variability in the Tropical Indian Ocean. *J. Climate*, **13**, 3487–3499.

Bishop, J.K.B., and W.B. Rossow, 1991: Spatial and temporal variability of global surface solar irradiance. *J. Geophys. Res.*, **96**, 16839–16858.

Chang, C.P., and T. Li, 2000: A theory for the tropical tropospheric biennial oscillation. *J. Atmos. Sci.*, **57**, 2209–2224.

Clark, C.O., J. E. Cole, and P.J. Webster, 2000: Indian Ocean SST and Indian summer Rainfall: Predictive Relinships a tr decalal variabilityiehdnoash. *J. Climate*, **13**, 2503–2519.

Darnell, W.L., W.F. Staylor, S.K. Gupta, N.A. Ritchey, and A.C. Wilber, 1992: Seasonal variation of surface radiation budget derived from ISCCP-C1 data. *J. Geophys. Res.*, **97**, 15741.

Fasullo, J.T., and P.J. Webster, 1999: Warm pool sea surface temperature variability in relations to the surface energy balance. *J. Climate*, **12**, 1292–1305.

Ferranti, L., J.M. Slingo, T.N. Palmer, and B.J. Hoskins, 1997: Relations between interannual and

intraseasonal monsoon variability as diagnosed from AMIP integrations. *Quart. J. Roy. Meteor. Soc.*, **123**, 1323–1327.

Garternicht, U., and F. Schott, 1997: Heat Fluxes of the Indian Ocean from a global eddy-resolving model. *J. Geophys. Res.*, **102**, 21147–21159.

Gill, A., 1982: *Atmosphere-Ocean Dynamics*, Vol. 30, *International Geophysics Series*. Academic Press, 662 pp.

Godfrey, J.S., A. Alexiou, A.G. Ilahude, D.M. Legler, M.E. Luther, J.P. McCreary, G.A. Meyers, K. Mizumo, R.R. Rao, S.R. Shetye, J.H. Toole, and S. Wacongne, 1995: The Role of the Indian Ocean in the Global Climate System: Recommendations Regarding the Global Ocean Observing System. Technical report, Ocean Observing System Development Panel, Texas A&M University, College Station, TX.

Han, W., and J.P. McCreary, 2001: Modeling salinity distributions in the Indian Ocean. *J. Geophys. Res.*, **106**, 859–877.

Harzallah, R., and R. Sadourny, 1997: Observed lead-lag realtionships between Indian summer monsoon and some meteorological variables. *Clim. Dyn.*, **13**, 635–648.

Hastenrath, S., 1987: On the meridional heat transports in the world ocean. *J. Clim. Appl. Meteorol.*, **26**, 847–857.

Hastenrath, S., and L. Greischar, 1993: The monsoonal heat budget of the hydrosphere-atmosphere system in the Indian Ocean sector. *J. Geophys. Res.*, **98**, 6869–6881.

Hsiung, J., R.E. Newell, and T. Houghtby, 1989: The annual cycle of oceanic heat storage and oceanic meridional heat transport. *Quart. J. Roy. Meteor. Soc.*, **115**, 1–28.

Jensen, T., 1993: Equatorial variability and resonance in a wind-driven Indian Ocean model. *J. Geophys. Res.*, **98**, 22533–22552.

Joseph, P.V., J.K. Eischeid, and R.J. Pyle, 1994: Interannual variability of the onset of the Indian summmer monsoon and its association with atmospheric features, El Niño, and sea surface temperature anomalies. *J. Climate*, **7**, 81–105.

Kalnay, E., M. Kanamitsu, R. Kistler, W. Collins, D. Deaven, L. Gandin, M. Iredell, S. Saha, G. White, J. Woollen, Y. Zhu, M. Chelliah, W. Ebisuzaki, W. Higgins, J. Janowiak, K.C. Mo, C. Ropelewski, J. Wang, A. Leetma, R Reynolds, R. Jenne, and D. Joseph, 1996: The NCEP/NCAR 40-Year Reanalysis Project. *Bull. Am. Meteor. Soc.*, **77**, 437–471.

Kindle, J.C., and J.D. Thompson, 1989: The 26- and 50-Day Oscillations in the Western Indian Ocean: Model Results. *J. Geophys. Res.*, **94**, 4721–4736.

Krishna Kumar, K., B. Rajagopalan, and M.A. Cane, 1999: On the weakening relationship between the Indian monsoon and ENSO. *Science*, **284**, 2156–2159.

Krishnamurti, T.N., H.S. Bedi, and M. Suramanian, 1989: The summer monsoon of 1987. *J. Climate*, **2**, 321–340.

Krishnamurti, T.N., H.S. Bedi, and M. Suramanian, 1990: The summer monsoon of 1988. *Meteor. Atmos. Phys.*, **42**, 19–37.

Lee, T., and J. Marotzke, 1997: Inferring meridional mass and heat transports of the Indian Ocean

by fitting a general circulation model to climatological data. *J. Geophys. Res.*, **102**, 10585–10602.

Levitus, S., 1987: Meridional Ekman heat fluxes for the world ocean and individual ocean basins. *J. Phys. Ocean.*, **17**, 1484–1492.

Loschnigg, J., and P.J. Webster, 2000: A coupled ocean-atmosphere system of SST modulation in the Indian Ocean. *J. Climate*, **13**, 3342–3360.

Luyten, J.R., and D.H. Roemmich, 1982: Equatorial curents at semi-annual period in the Indian Ocean. *J. Phys. Ocean.*, **12**, 406–413.

Matsuno, T., 1966: Quasi-geostrophic motions in the equatorial area. *J. Met. Soc. Japan*, **44**, 25–43.

McCreary, Jr., J.P., P.K. Kundu, and R.L. Molinari, 1993: A numerical investigation of dynamics, thermodynamics and mixed-layer processes in the Indian Ocean. *Prog. Oceanog.*, **31**, 181–244.

Meehl, G.A., 1987: The annual cycle and interannual variability in the tropical Pacific and Indian ocean regions. *Mon. Wea. Rev.*, **115**, 27–50.

Meehl, G.A., 1993: A coupled air-sea biennial mechanism in the tropical Indian and Pacific ocean regions: Role of the ocean. *J. Climate*, **6**, 31–41.

Meehl, G.A., 1997: The South Asian Monsoon and the Tropospheric Biennial Oscillation. *J. Climate*, **10**, 1921–1943.

Meehl, G.A., and J.M. Arblaster, 2001: The tropospheric biennial oscillation and Asian-Australian monsoon rainfall. Submitted to *J. Climate*.

Mooley, D.A., and B. Parthasarathy, 1984: Fluctuations in all-India summer monsoon rainfall during 1871-1978. *Clim. Change*, **6**, 287–301.

Moore, D.W., and J.P. McCreary, 1990: Excitation of intermediate-frequency equatorial waves at a western ocean boundary: With application to observations from the Indian Ocean. *J. Geophys. Res.*, **95**, 5219–5231.

Murtugudde, R., and A.J. Busalacci, 1999: Interannual variability of the dynamics and thermodynamics of the tropical Indian Ocean. *J. Climate*, **12**, 2300–2326.

Nicholls, N., 1989: Sea surface temperatures and Australian winter rainfall. *J. Climate*, **2**, 965–973.

Palmer, T.N., 1993: Extended range atmospheric prediction and the Lorenz model. *Bull. Am. Meteor. Soc.*, **74**, 49–65.

Palmer, T.N., 1994: Chaos and predictability in forecasting the monsoons. *Proc. Indian Natn. Sci. Acad.*, **60**, 57–66. Part A.

Palmer, T.N., C. Brankovich, P. Viterbo, and M.J. Miller, 1992: Modelling interannual variations of summer monsoons. *J. Climate*, **5**, 399–417.

Palmer, T.N., and D.A. Mansfield, 1984: Response of two atmospheric general circulation models to sea-surface temperature anomalies in the tropical east and west pacific. *Nature*, **310**, 483–485.

Parthasarathy, B., K. Rupa Kumar, and D. R. Kothawale, 1992: Indian summer monsoon rainfall indices. *Meteorol. Mag.*, **121**, 174–186.

Rasmusson, E.M., and T.H. Carpenter, 1983: The relationship between eastern equatorial Pacific sea surface temperatures and rainfall over Indian and Sri Lanka. *Mon. Wea. Rev.*, **111**, 517–528.

Reason, C.J.C., R.J. Allan, J.A. Lindesay, and T.J. Ansell, 2000: ENSO and climatic signals across the Indian Ocean Basin in the global context: Part 1. Interannual composite patterns. *Int. J. Climatol.*, **20**, 1285–1387.

Reppin, J., F. Schott, and J. Fisher, 1999: Equatorial currents and transports in the upper-central Indian Ocean: Annual cycle and interannual variability. *J. Geophys. Res.*, **104**, 15495–15514.

Reverdin, G., and J. Luyten, 1986: Near-surface meanders in the equatorial Indian Ocean. *J. Phys. Ocean.*, **16**, 1088–1100.

Reynolds, R.W., and T.M. Smith, 1994: Improved global sea surface temperature analyses using optimum interpolation. *J. Climate*, **7**, 929–948.

Rodwell, M.J., 1998: Breaks in the asian monsoon: the influence of the southern hemisphere weather systems. *J. Atmos. Sci.*, **54**, 2597–2611.

Sadhuram, Y., 1997: Predicting monsoon rainfall and pressure indecies from sea surface temperature. *Current Science*, **72**, 166–168.

Saji, N.H., B.N. Goswami, P.N. Vinayachandran, and T. Yamagata, 1999: A dipole mode in the Indian Ocean. *Nature*, **401**, 360–363.

Saji, N.H., B.N. Goswami, P.N. Vinayachandran, and T. Yamagata, 1999: A dipole mode in the tropical Indian Ocean. *Nature*, **401**, 360–363.

Shukla, J., and D.A. Paolino, 1983: The Southern Oscillation and long-range forecasting of the summer monsoon rainfall over India. *Mon. Wea. Rev.*, **111**, 1830–1837.

Torrence, C., and G.P. Compo, 1998: A Practical Guide to Wavelet Analysis. *Bull. Am. Meteor. Soc.*, **79**, 61–78.

Torrence, C., and P.J. Webster, 1998: The annual cycle of persistence in the El Niño-Southern Oscillation. *Quart. J. Roy. Meteor. Soc.*, **124**, 1985–2004.

Torrence, C., and P.J. Webster, 1999: Interdecadal changes in the ENSO-Monsoon System. *J. Climate*, **12**, 2679–2690.

Tsai, P.T.H., J.J. O'Brien, and M.E. Luther, 1992: The 26-day oscillation observed in the satellite sea surface temperature measurements in the equatorial western Indian Ocean. *J. Geophys. Res.*, **97**, 9605–9618.

Vernekar, A.D., J. Zhou, and J. Shukla, 1995: The effect of Eurasian snow cover in the Indian monsoon. *J. Climate*, **8**, 248–266.

Wacongne, S., and R.C. Pacanowski, 1996: Seasonal heat transport in the tropical Indian Ocean. *J. Phys. Ocean.*, **26**(12), 2666–2699.

Webster, P.J., 1994: The role of hydrological processes in ocean-atmosphere interactions. *Rev. Geophys.*, **32**, 427–476.

Webster, P.J., and R. Lukas, 1992: TOGA COARE: The Coupled Ocean-Atmosphere Response Experiment. *Bull. Am. Meteor. Soc.*, **73**, 1377–1416.

Webster, P.J., V. Magana, T.N. Palmer, J. Shukla, R. Tomas, T.M. Yanai, and T. Yasunari, 1998: The Monsoon: Processes, Predictability and the Prospects for Prediction. *J. Geophys. Res.*, **103**, 14,451.

Webster, P.J., A. Moore, J.P. Loschnigg, and R. Leben, 1999: Coupled ocean-atmosphere dynamics in the Indian Ocean during 1997-1998. *Nature*, **401**, 356–360.

Webster, P.J., and S. Yang, 1992: Monsoon and ENSO: Selectively interactive systems. *Quart. J. Roy. Meteor. Soc.*, **118**, 877–926.

Woodberry, K.E., M.E. Luther, and J.J. O'Brien, 1989: The wind-driven seasonal circulation in the southern tropical Indian Ocean. *J. Geophys. Res.*, **94**, 17985–18002.

Yasunari, T., 1991: The monsoon year - a new concept of the climatic year in the tropics. *Bull. Am. Meteor. Soc.*, **72**, 1331–1338.

Yasunari, T., A. Kitoh, and T. Tokioka, 1991: Local and remote reponses to excessive snow mass over Eurasia appearing in the northern spring and summer climate: A study with the MRI-GCM. *J. Met. Soc. Japan*, **69**, 473–487.

Figure 1: A) Annual mean heat transport vs. Latitude for the climatological forcing in Loschnigg and Webster 2000 (LW), compared with values obtained by Levitus 1987, Hsiung *et al.* 1989, Hastenrath and Greischar 1993 (HG), Garternicht and Schott 1997 (GS) and Wacongne and Pacanowski 1996 (WP). Values given in PW (1PW = 10^{15} W). Positive values indicate northward heat transport, and negative values indicate southward heat transport. Adapted from Garternicht and Schott (1997), Wacongne and Pacanowski (1996) and Loschnigg and Webster (2000). B) Schematic of the annual cycle of the heat balance for the Indian Ocean as simulated in a $2\frac{1}{2}$ layer ocean model (adapted from Loschnigg and Webster 2000).

Figure 2: Model T_m for JJA of a) 1987 and b) 1988. Reynolds SST for JJA of c) 1987 and d) 1988.

Figure 3: Timeseries of the anomalies (annual and semi-annual cycles removed) of Reynolds SST and model T_m for the a) North and b) South Indian Ocean for the years 1987 and 1988. Solid line is model T_m, dashed line is Reynolds SST. Correlations (r^2) are given for the anomalies of Reynolds SST and model T_m from 1984 to 1990.

Figure 4: Hovmöller diagram of model layer 1 meridional velocity for 1987 and 1988 along the equator. Contours in $\pm$ 0.1 ms^{-1}. Positive contour lines are solid, negative contour lines are dashed.

Figure 5: Differences between 1988 and 1987 JJA winds ($msec^{-1}$). Arrows show the vector differences of the directional wind speeds for 1988 minus 1987. Color contours show the differences in scalar wind speed magnitudes for 1988 minus 1987, with positive contours indicating higher windspeeds for 1988 compared to 1987, negative contours indicating lower windspeeds in 1988.

Figure 6: Hovmöller diagram of model equatorial u_1, with contours of $\pm$ 0.2 ms^{-1}. Positive contour lines are solid, negative contour lines are dashed. See text for description of lines $A - A'$ and $B - B'$.

Figure 7: Annual mean model heat transport (Q_v) as a function of latitude for the years 1984-1990. Values given in PW (1 PW = 10^{15} W).

Figure 8: Components of the total heat transport ($Q_{v(TOT)}$, $Q_{v(EK)}$, $Q_{v(G)}$) for the 1984-1990 climatology for a) Annual mean, b) Jun - Aug, and c) Jan - Feb. Units in PW.

Figure 9: Meridional heat transport (PW) plotted against the zonal mean of the zonal wind ($msec^{-1}$) for the climatological annual cycle, analyzed along latitude lines at a) 15°N, b) 10°N, c) 5°S, d) 10°S and e) 15°S.

Figure 10: Model Ekman heat transport ($Q_{v(EK)}$) as a function of latitude for the years 1987, 1988 and for the 1984-1990 climatology. Values given for a) Annual mean, b) Jun - Aug, and c) Jan - Feb. Note that the horizontal scale of plot b) (Jun - Aug) is enlarged compared to the others. Units PW.

Figure 11: Power Hovmöller diagrams of model (a) mixed layer temperature (T_m) and (b) mixed layer depth (h_m) for points along the equator. Wavelets of each field were taken every 2° along the Equator from 46°to 92°E. Wavelet power was then averaged between periods of 10 to 60 days according to Torrence and Compo (1998). Contours are in normalized percent variance relative to white noise. Thick solid line is the 95% significance level.

Figure 12: Wavelet power spectrum of model equatorial layer 1 (a) meridional (v_1) and (b) zonal (u_1) velocity at 80°E. Both time series are anomalies from the annual cycle. Contours are in units of normalized variance. Curved solid line represents the "cone of influence", above which values may not be accurate due to the limited temporal span of the time series. Thick solid contours represents the 95% significance level.

Figure 13: Power Hovmöllers of model equatorial layer 1 (a) meridional (v_1) and (b) zonal (u_1) velocity. As in Fig. 11, but with averaging periods of (a) 10-60 days and (b) 100-250 days. Contours are in normalized percent variance relative to white noise. Thick solid line is the 95% significance level.

Figure 14: Wavenumber/frequency spectrum of model equatorial v_1. The horizontal axis has units of planetary wave number s, where $k = \frac{2\pi s}{L}$ and L is the equatorial circumference. Negative wavenumber corresponds to westward phase speed, and positive wavenumber corresponds to eastward phase speed. Contours in units of percent variance of $(ms^{-1})^2$. Vertical dashed lines correspond to planetary wavenumbers lower than 4.5, which cannot be resolved due to the limited zonal scale of the Indian Ocean basin. The curved line corresponds to the dispersion curve for the equatorial $n = 0$ mixed Rossby-gravity (Yanai) wave with an equivalent depth $H_e = 0.13m$ (Gill 1982). It should be noted that the vertical scale is expanded so as to show only a partial section of the full wavenumber-frequency spectrum as depicted by Gill (1982).

Figure 15: Model layer 1 current vectors for (a) Aug. 13 and (b) Aug. 18 1984 for the central Indian Ocean. Also shown is the zero absolute vorticity line.

Figure 16: Wavenumber/frequency spectrum of model equatorial u_1. Axes as in Fig. 14. Contours in units of percent variance of $(ms^{-1})^2$. Vertical dashed lines correspond to planetary wavenumbers lower than 4.5, which cannot be resolved. The curved line on the left of the diagram corresponds to the dispersion curve for the equatorial $n = 1$ Rossby wave with an equivalent depth $H_e = 0.13m$. The line on the right corresponds to the dispersion curve for the equatorial $n = 1$ Kelvin wave with a similar equivalent depth (Gill 1982).

Figure 17: A possible biennial cycle of heat transport and SST anomalies for the northern Indian Ocean. The cycle arbitrarily starts at the uppermost panel (a), with a "strong" monsoon year. Curved black arrows denote the wind forced by the large-scale differential heating denoted by the warm (red) and cool (blue) hemispheres. The small yellow arrows are the Ekman transports forced by the winds, which are to the south on both sides of the equator. The resulting strong southward heat transports leave the northern Indian Ocean with cool SST anomalies (b), which contribute to the development of a "weak" monsoon the following boreal summer (c), depicted by weaker surface winds and weaker Ekman heat transports. The weak Ekman transports leave the northern Indian Ocean with warm SST anomalies (d), which contribute to a "strong" monsoon the following boreal summer (a).

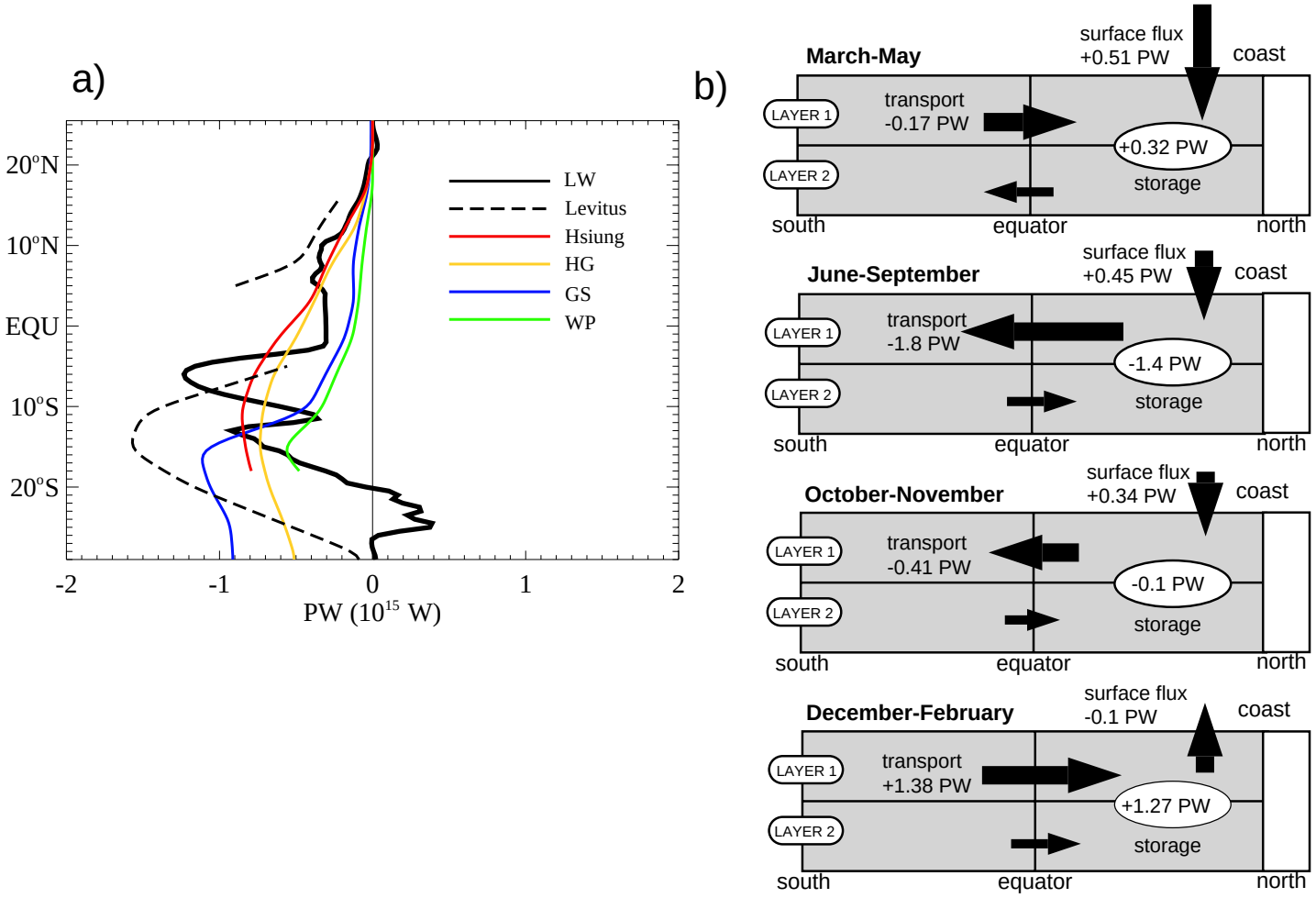

Figure 1: A) Annual mean heat transport vs. Latitude for the climatological forcing in Loschnigg and Webster 2000 (LW), compared with values obtained by Levitus 1987, Hsiung *et al.* 1989, Hastenrath and Greischar 1993 (HG), Garternicht and Schott 1997 (GS) and Wacongne and Pacanowski 1996 (WP). Values given in PW (1PW = 10^{15} W). Positive values indicate northward heat transport, and negative values indicate southward heat transport. Adapted from Garternicht and Schott (1997), Wacongne and Pacanowski (1996) and Loschnigg and Webster (2000). B) Schematic of the annual cycle of the heat balance for the Indian Ocean as simulated in a $2\frac{1}{2}$ layer ocean model (adapted from Loschnigg and Webster 2000).

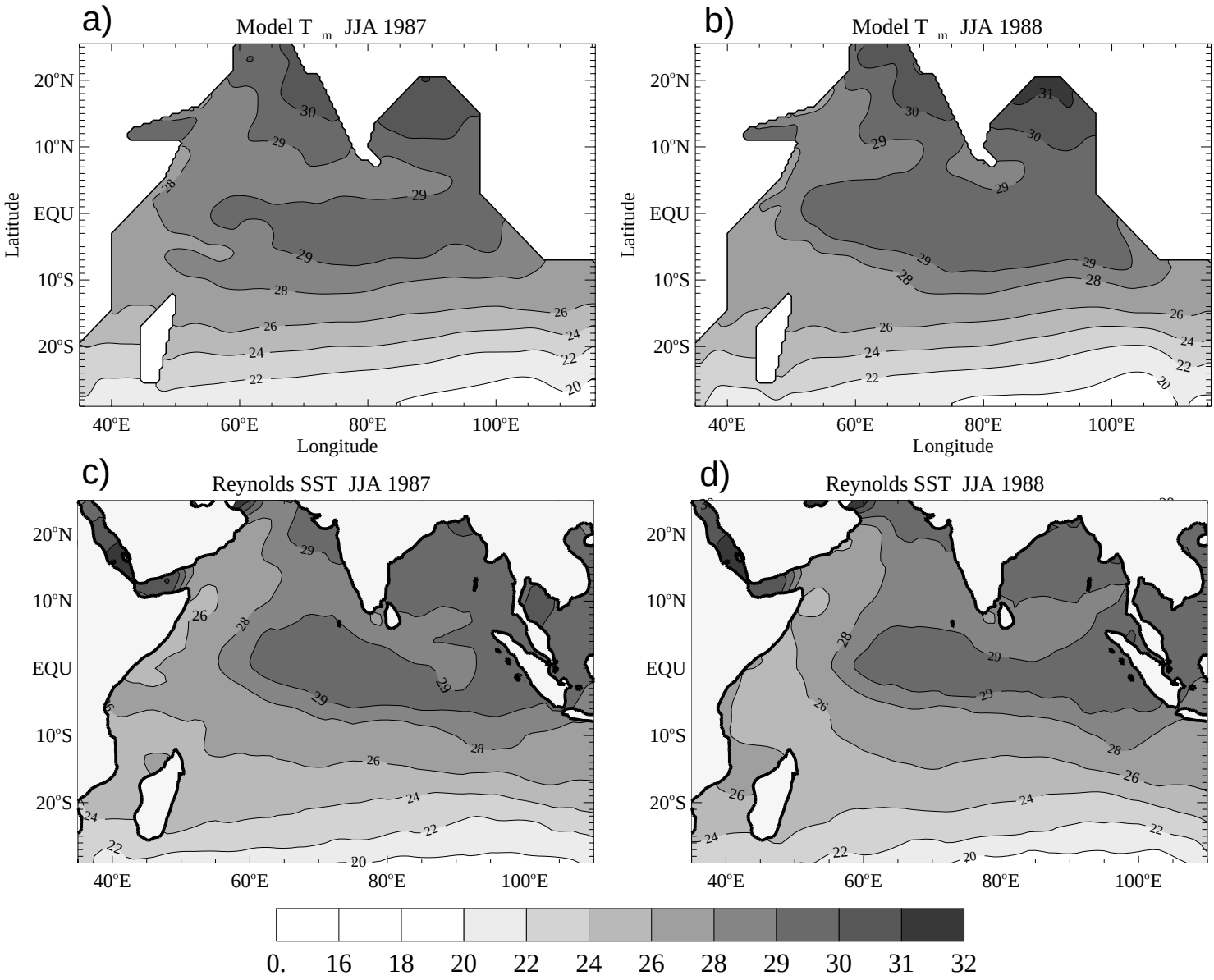

Figure 2: Model T_m for JJA of a) 1987 and b) 1988. Reynolds SST for JJA of c) 1987 and d) 1988.

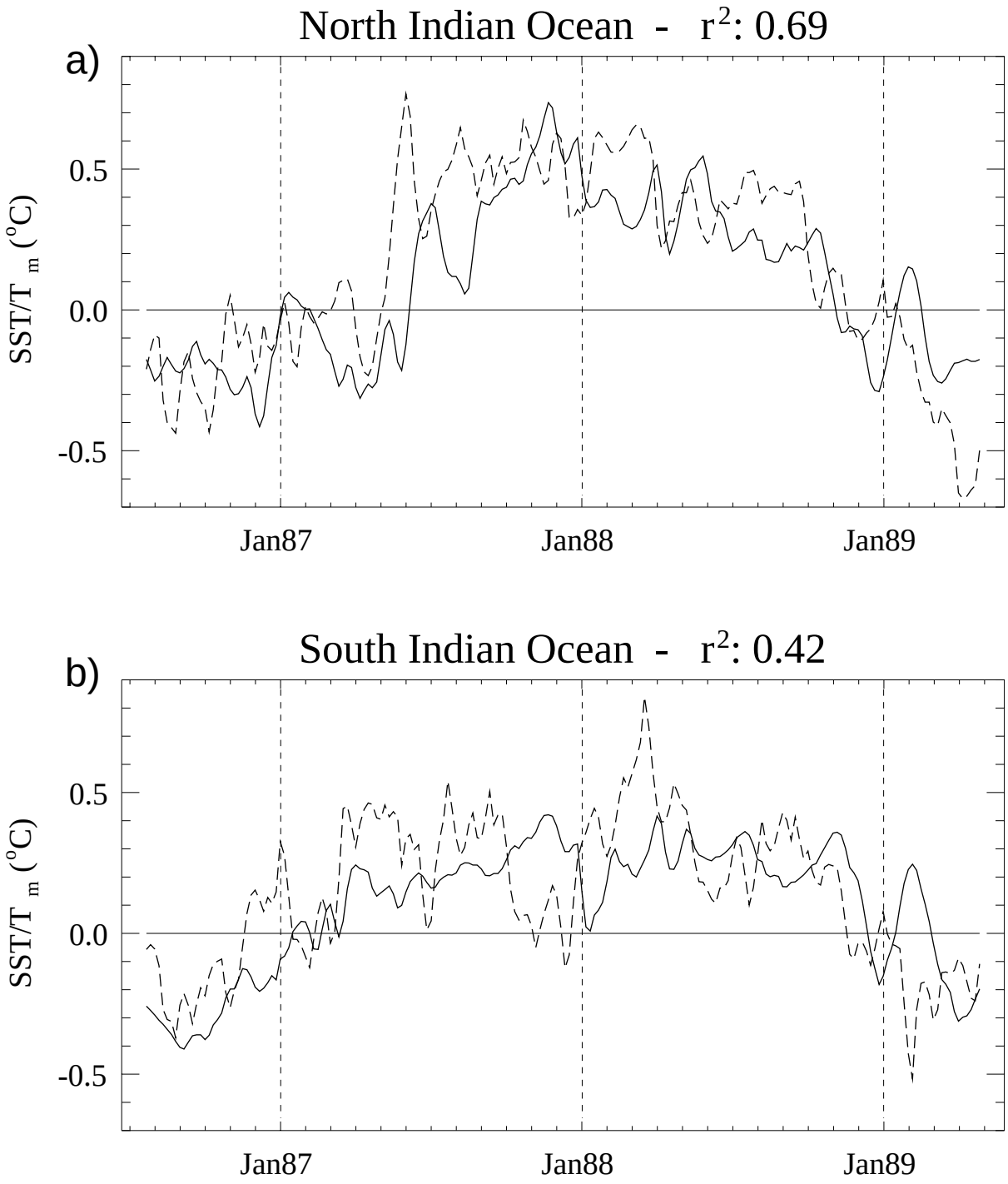

Figure 3: Timeseries of the anomalies (annual and semi-annual cycles removed) of Reynolds SST and model T_m for the a) North and b) South Indian Ocean for the years 1987 and 1988. Solid line is model T_m, dashed line is Reynolds SST. Correlations (r^2) are given for the anomalies of Reynolds SST and model T_m from 1984 to 1990.

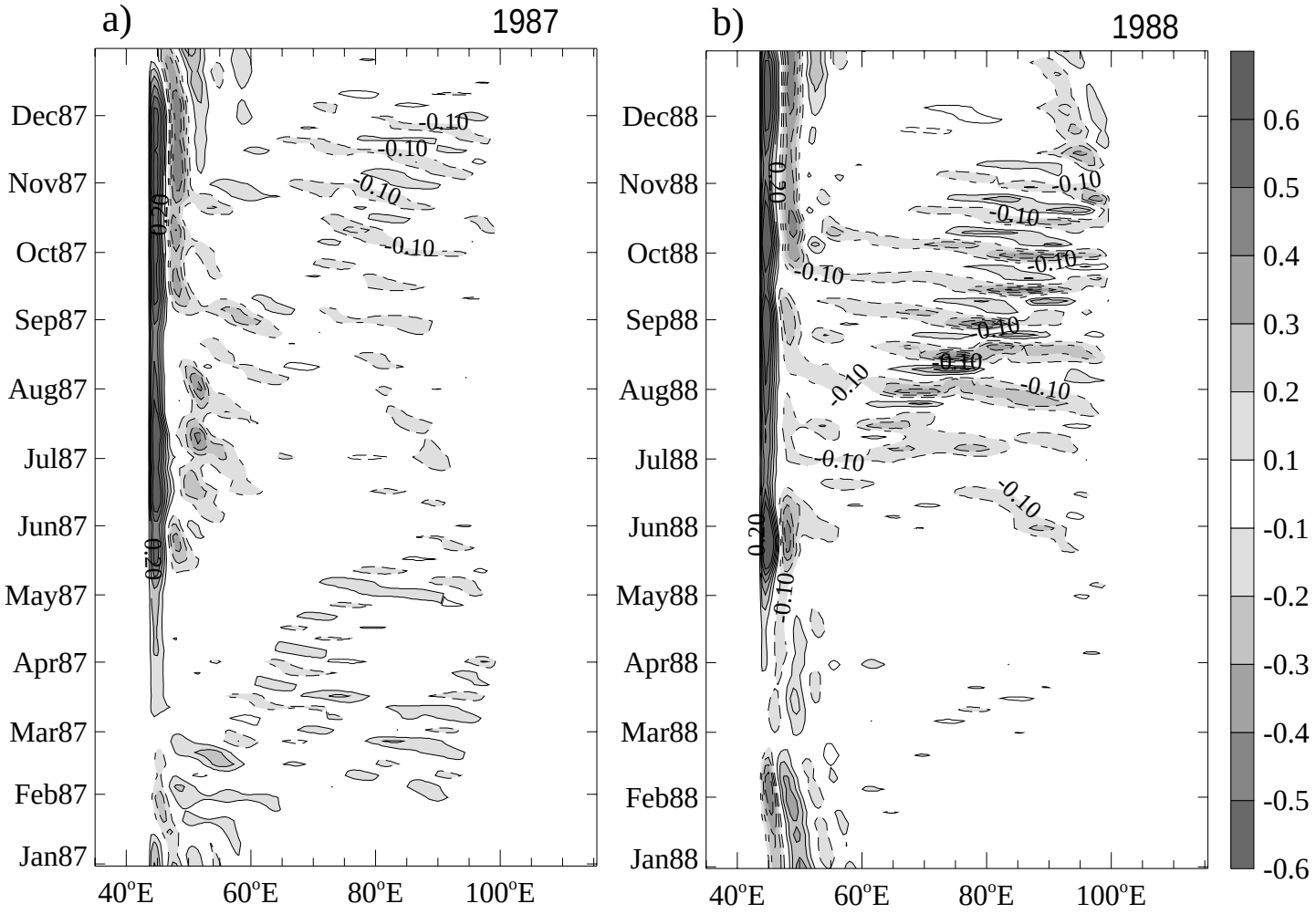

Figure 4: Hovmöller diagram of model layer 1 meridional velocity for 1987 and 1988 along the equator. Contours in $\pm$ 0.1 ms^{-1}. Positive contour lines are solid, negative contour lines are dashed.

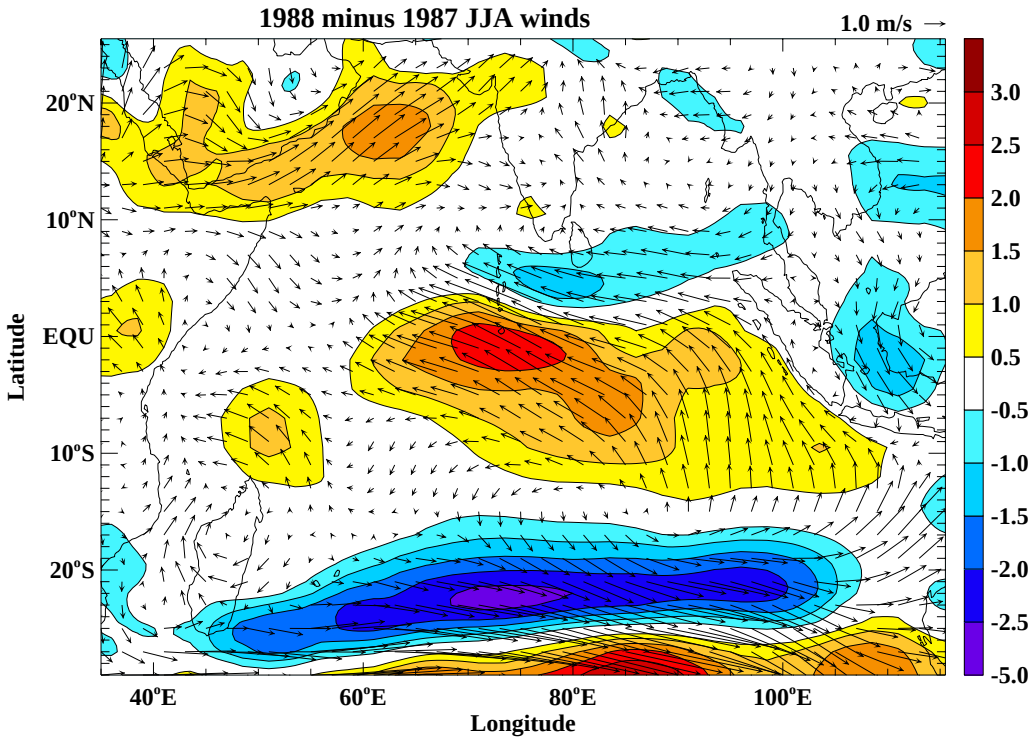

Figure 5: Differences between 1988 and 1987 JJA winds ($msec^{-1}$). Arrows show the vector differences of the directional wind speeds for 1988 minus 1987. Color contours show the differences in scalar wind speed magnitudes for 1988 minus 1987, with positive contours indicating higher windspeeds for 1988 compared to 1987, negative contours indicating lower windspeeds in 1988.

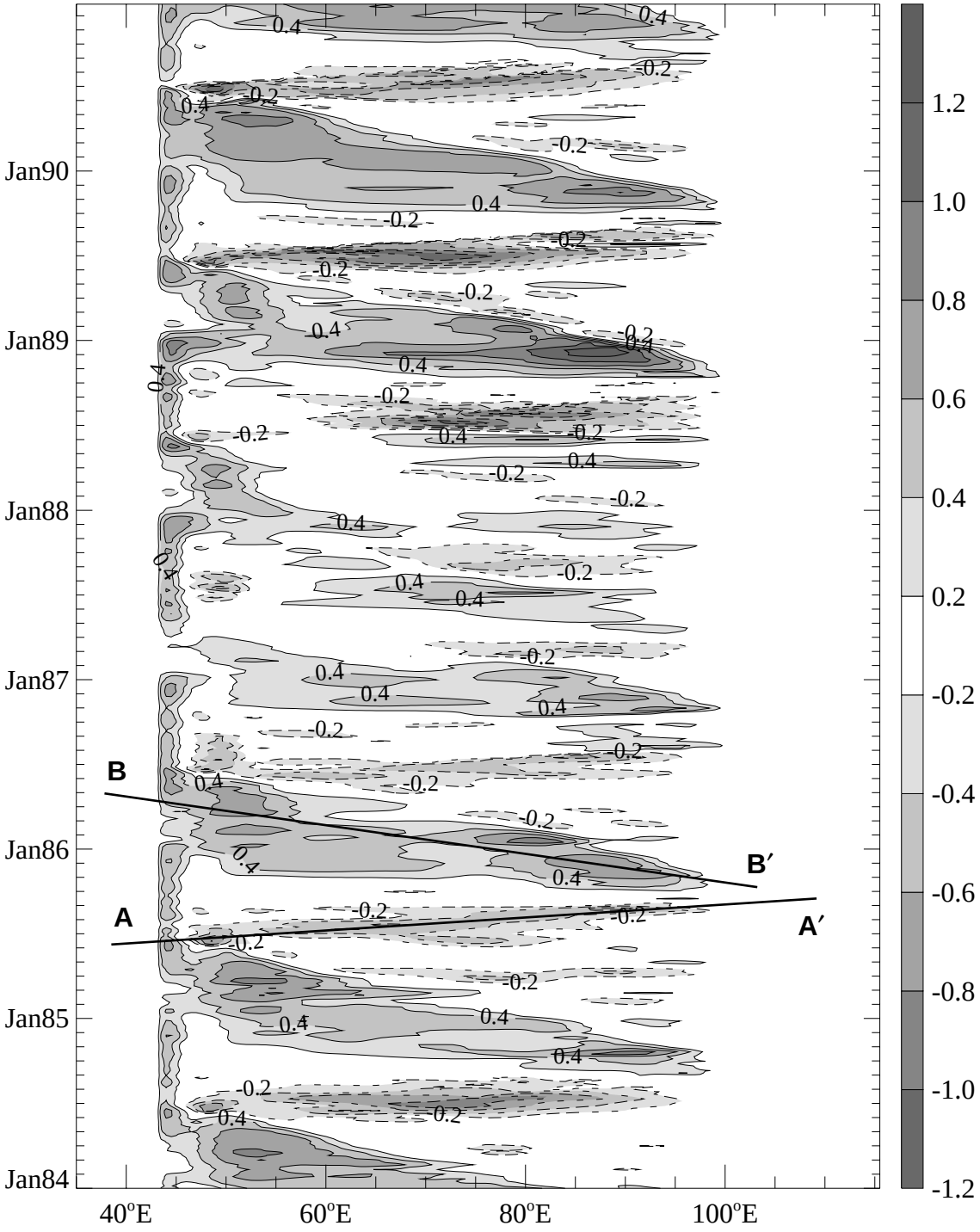

Figure 6: Hovmöller diagram of model equatorial u_1, with contours of $\pm$ 0.2 ms^{-1}. Positive contour lines are solid, negative contour lines are dashed. See text for description of lines $A - A'$ and $B - B'$.

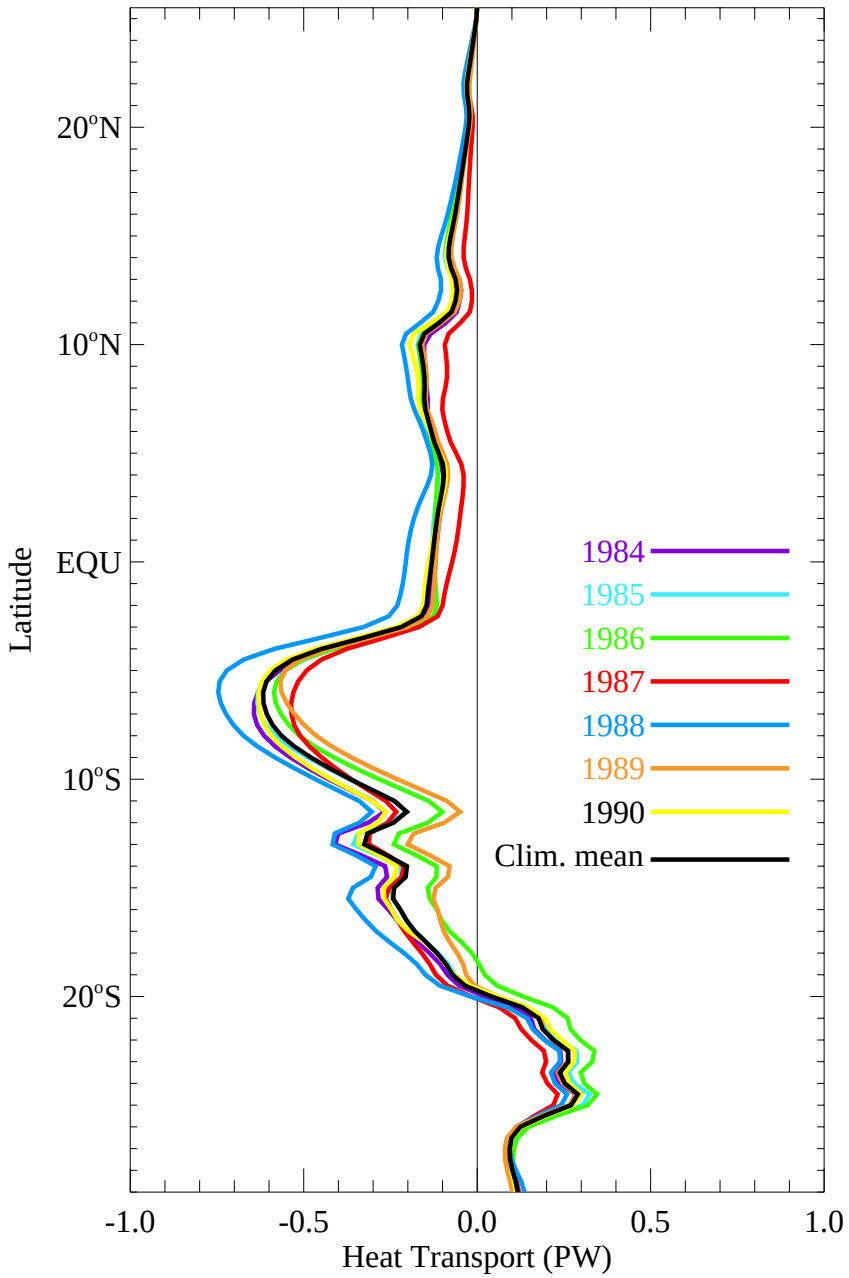

Figure 7: Annual mean model heat transport (Q_v) as a function of latitude for the years 1984-1990. Values given in PW (1 PW = 10^{15} W).

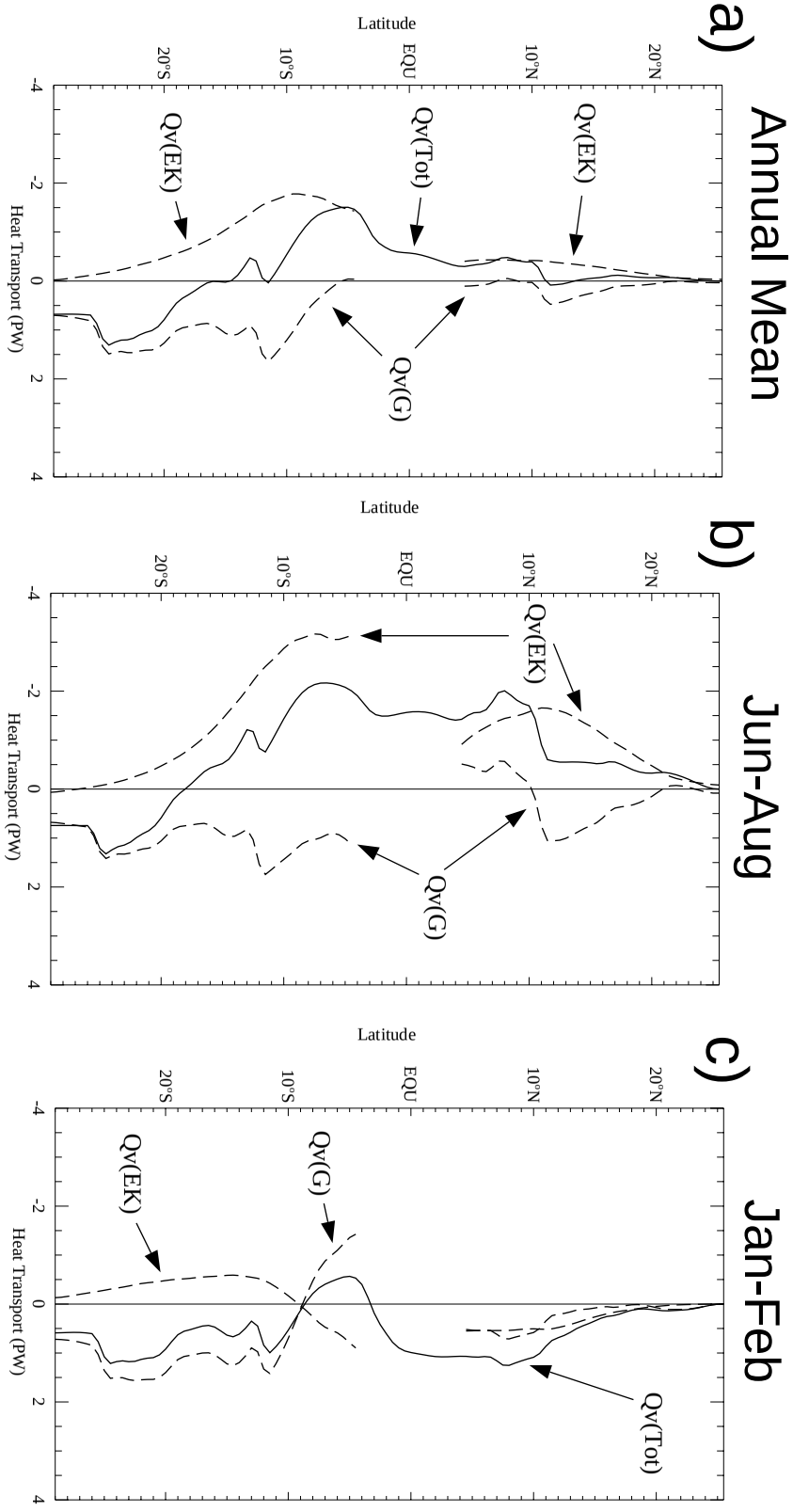

Figure 8: Components of the total heat transport ($Q_{v(TOT)}$, $Q_{v(EK)}$, $Q_{v(G)}$) for the 1984-1990 climatology for a) Annual mean, b) Jun - Aug, and c) Jan - Feb. Units in PW.

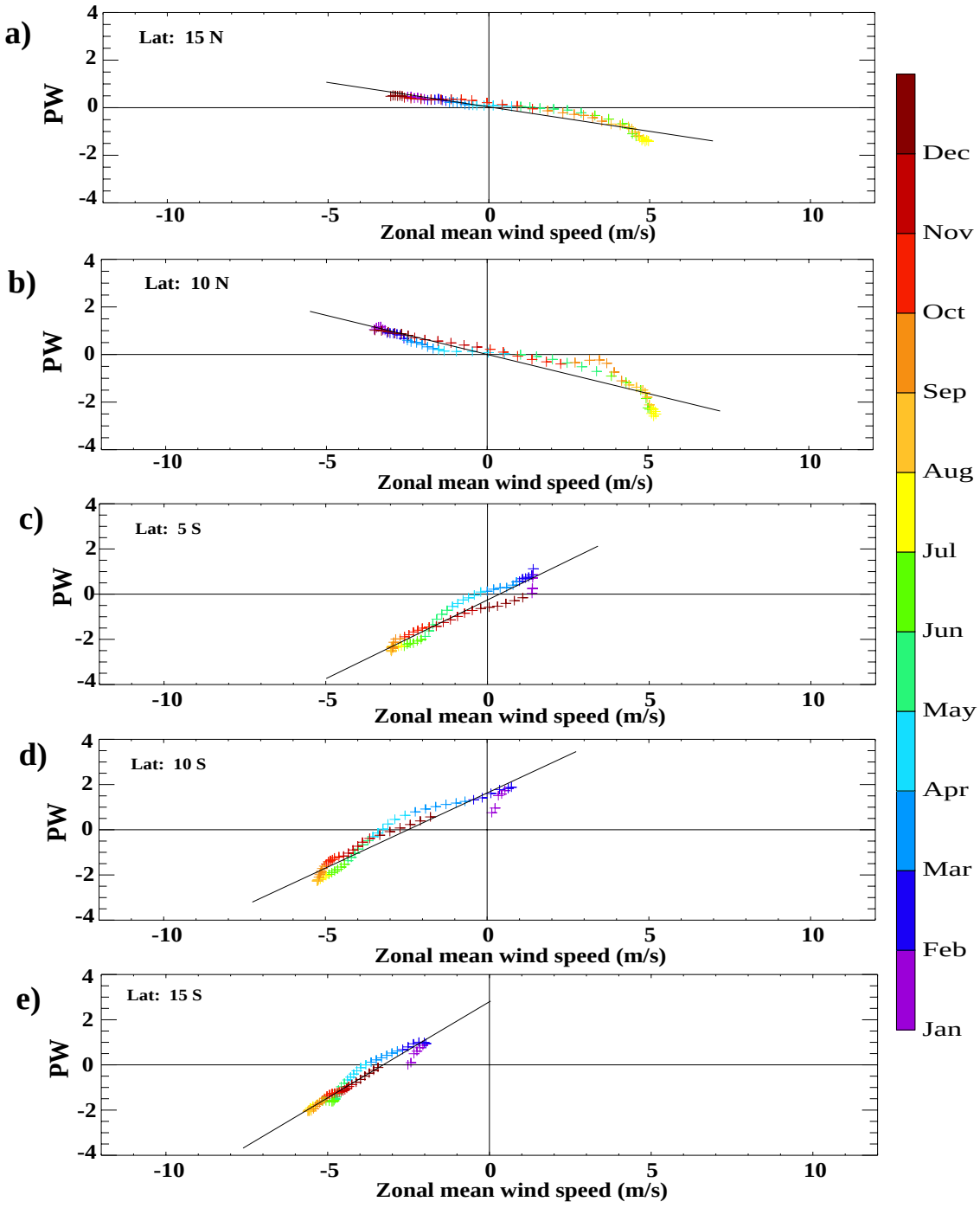

Figure 9: Meridional heat transport (PW) plotted against the zonal mean of the zonal wind ($msec^{-1}$) for the climatological annual cycle, analyzed along latitude lines at a) 15°N, b) 10°N, c) 5°S, d) 10°S and e) 15°S.

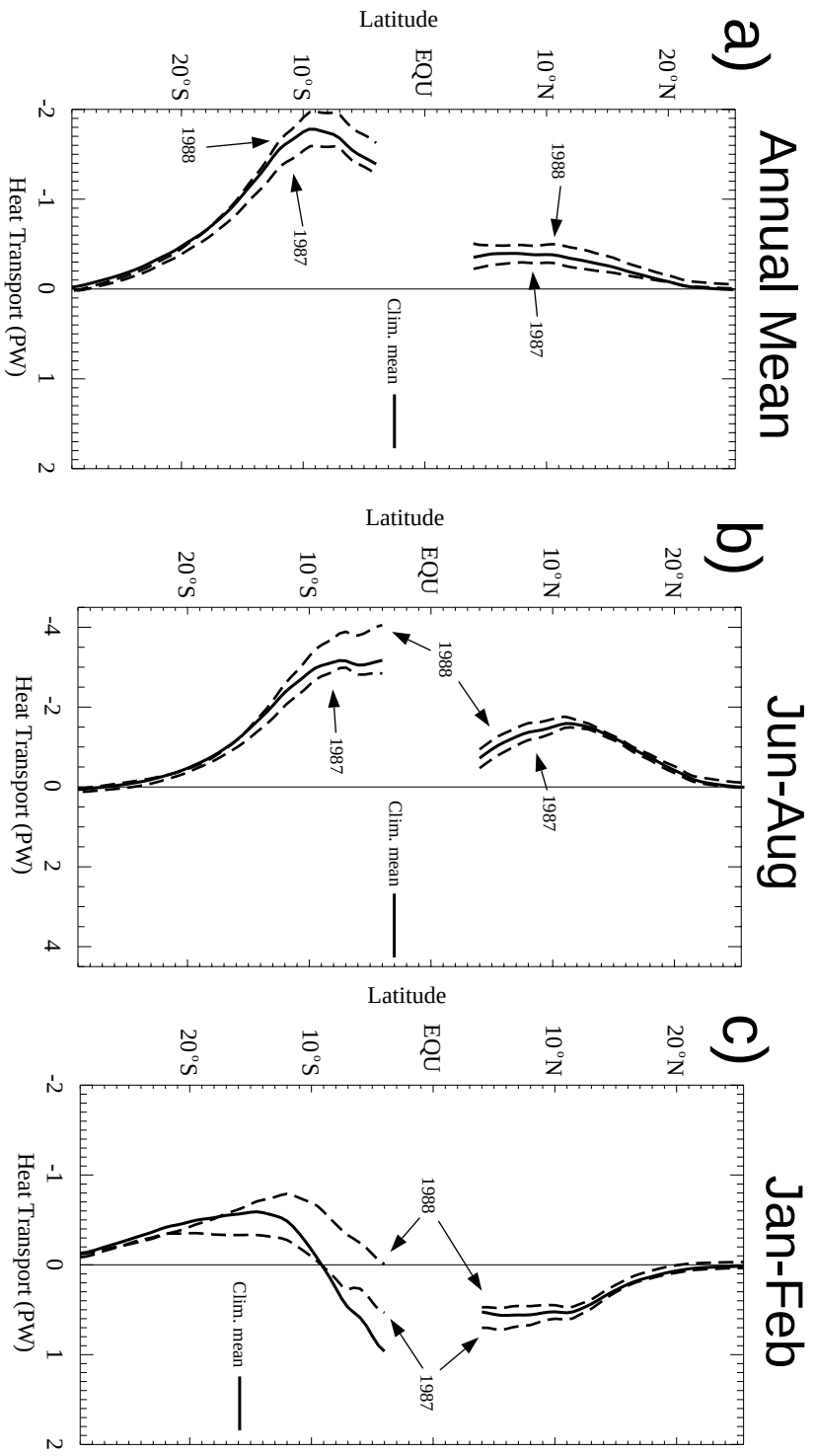

Figure 10: Model Ekman heat transport ($Q_{v(EK)}$) as a function of latitude for the years 1987, 1988 and for the 1984-1990 climatology. Values given for a) Annual mean, b) Jun - Aug, and c) Jan - Feb. Note that the horizontal scale of plot b) (Jun - Aug) is enlarged compared to the others. Units PW.

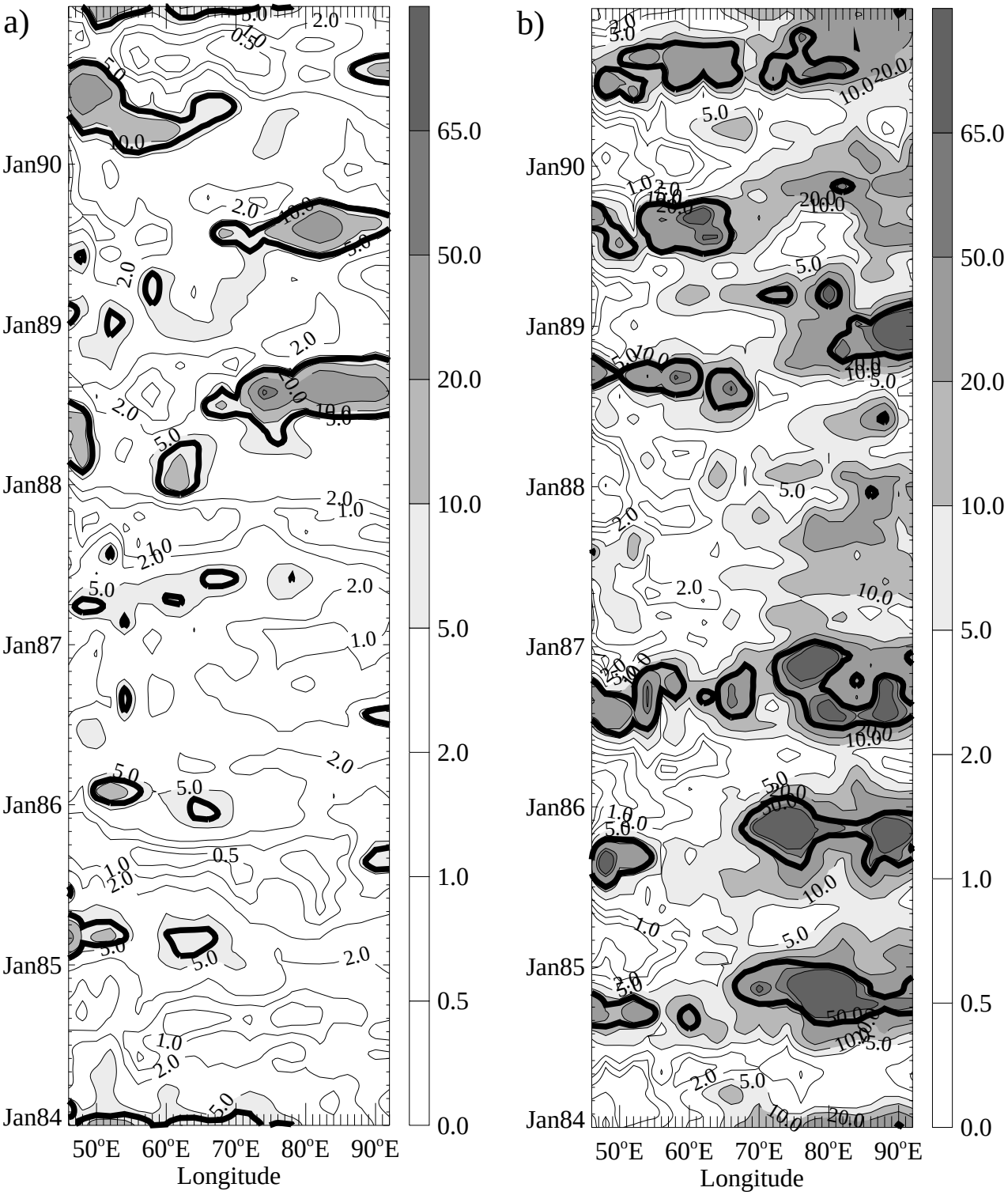

Figure 11: Power Hovmöller diagrams of model (a) mixed layer temperature (T_m) and (b) mixed layer depth (h_m) for points along the equator. Wavelets of each field were taken every 2° along the Equator from 46° to 92°E. Wavelet power was then averaged between periods of 10 to 60 days according to Torrence and Compo (1998). Contours are in normalized percent variance relative to white noise. Thick solid line is the 95% significance level.

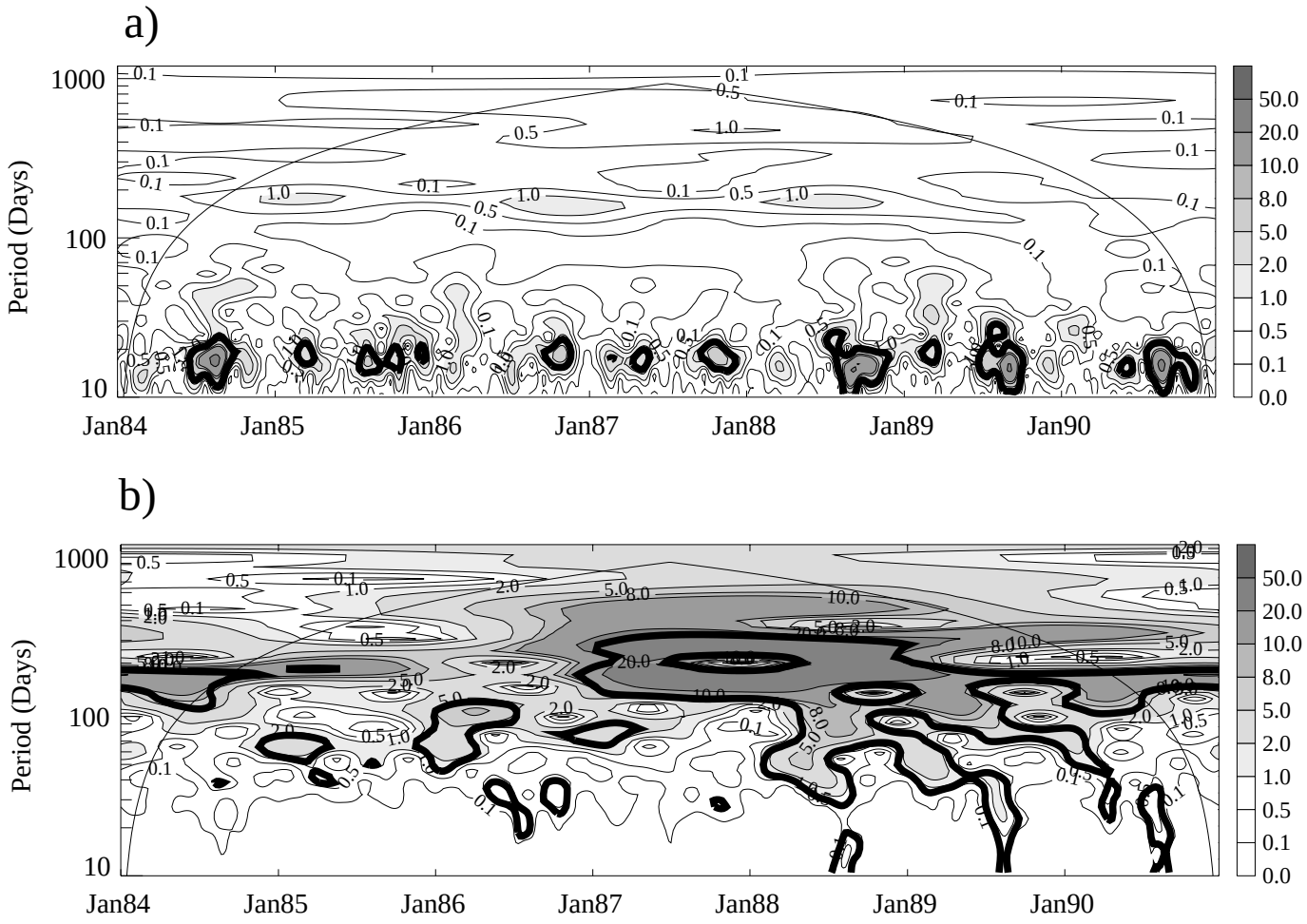

Figure 12: Wavelet power spectrum of model equatorial layer 1 (a) meridional (v_1) and (b) zonal (u_1) velocity at 80°E. Both time series are anomalies from the annual cycle. Contours are in units of normalized variance. Curved solid line represents the "cone of influence", above which values may not be accurate due to the limited temporal span of the time series. Thick solid contours represents the 95% significance level.

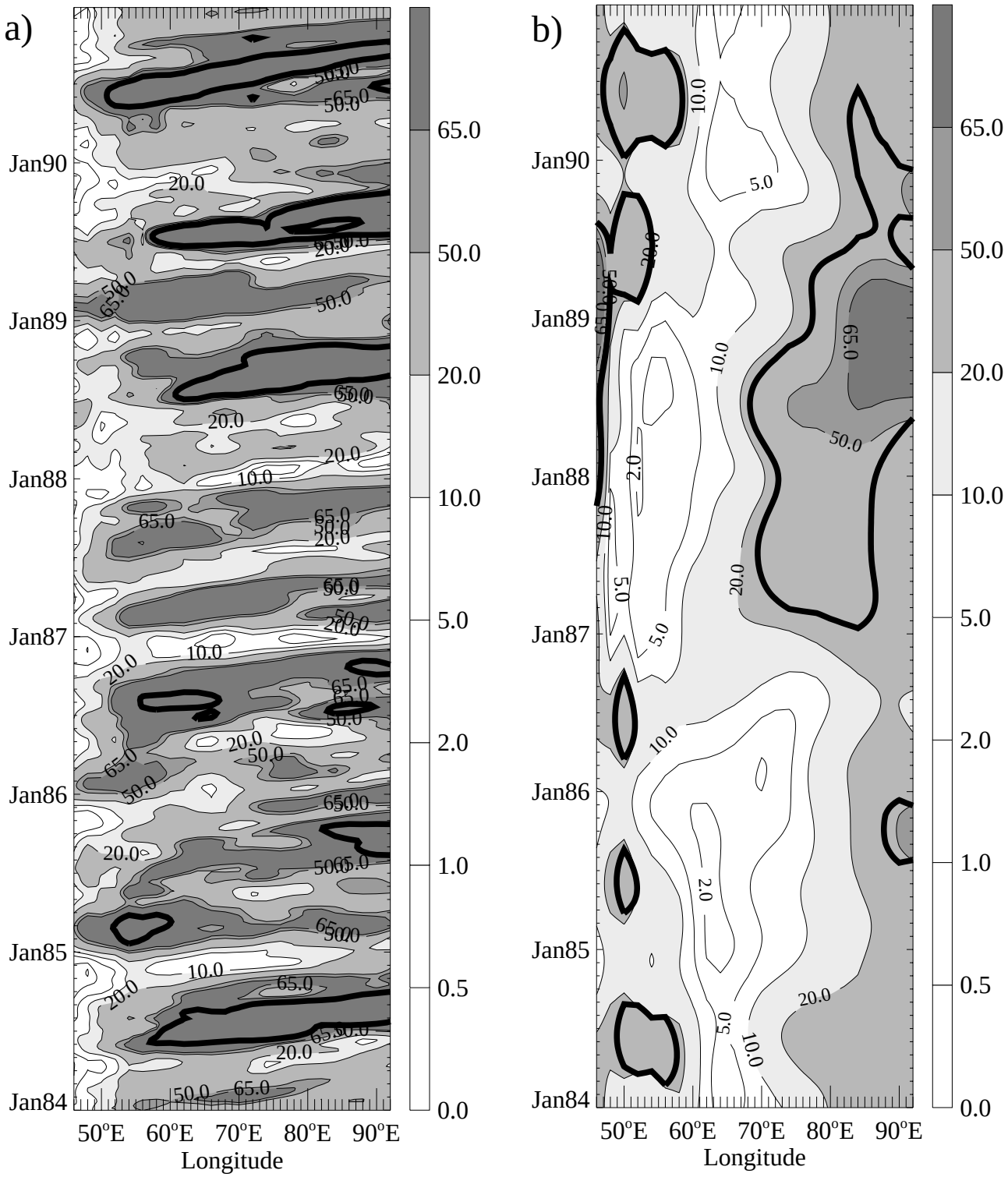

Figure 13: Power Hovmöllers of model equatorial layer 1 (a) meridional (v_1) and (b) zonal (u_1) velocity. As in Fig. 11, but with averaging periods of (a) 10-60 days and (b) 100-250 days. Contours are in normalized percent variance relative to white noise. Thick solid line is the 95% significance level.

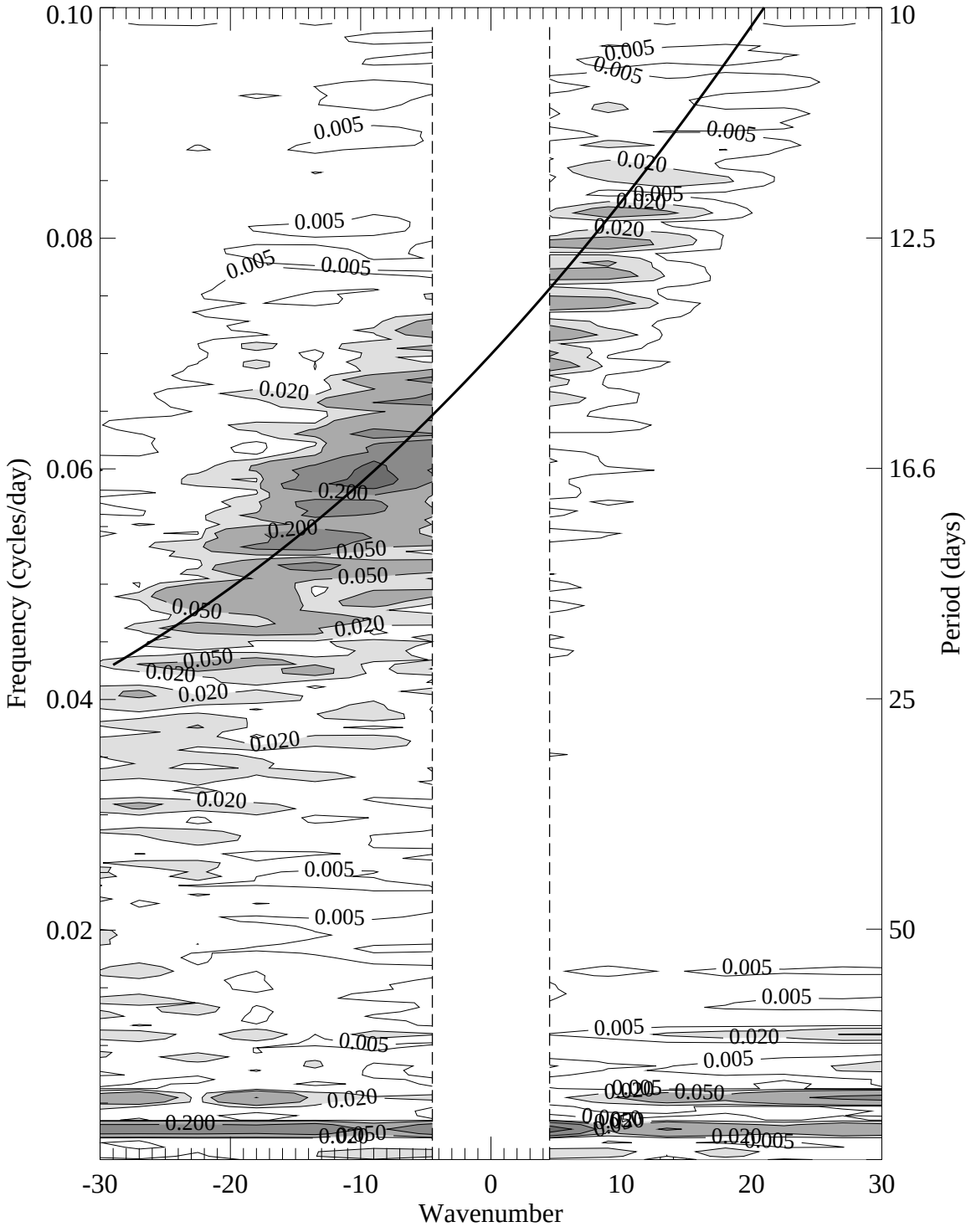

Figure 14: Wavenumber/frequency spectrum of model equatorial v_1. The horizontal axis has units of planetary wave number s, where $k = \frac{2\pi s}{L}$ and L is the equatorial circumference. Negative wavenumber corresponds to westward phase speed, and positive wavenumber corresponds to eastward phase speed. Contours in units of percent variance of $(ms^{-1})^2$. Vertical dashed lines correspond to planetary wavenumbers lower than 4.5, which cannot be resolved due to the limited zonal scale of the Indian Ocean basin. The curved line corresponds to the dispersion curve for the equatorial $n = 0$ mixed Rossby-gravity (Yanai) wave with an equivalent depth $H_e = 0.13m$ (Gill 1982). It should be noted that the vertical scale is expanded so as to show only a partial section of the full wavenumber-frequency spectrum as depicted by Gill (1982).

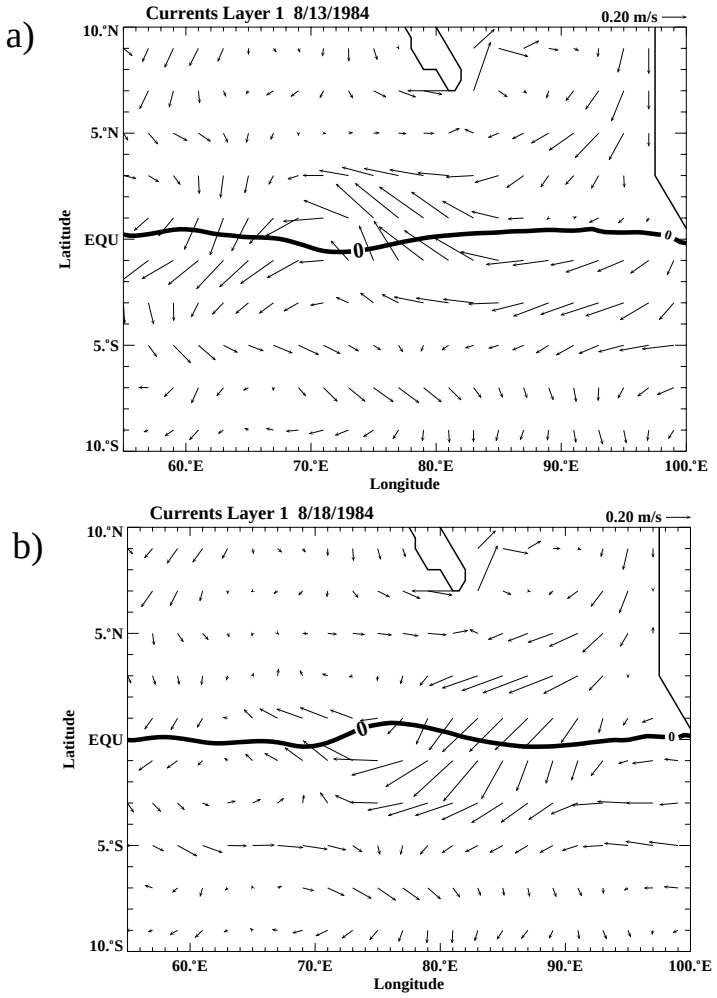

Figure 15: Model layer 1 current vectors for (a) Aug. 13 and (b) Aug. 18 1984 for the central Indian Ocean. Also shown is the zero absolute vorticity line.

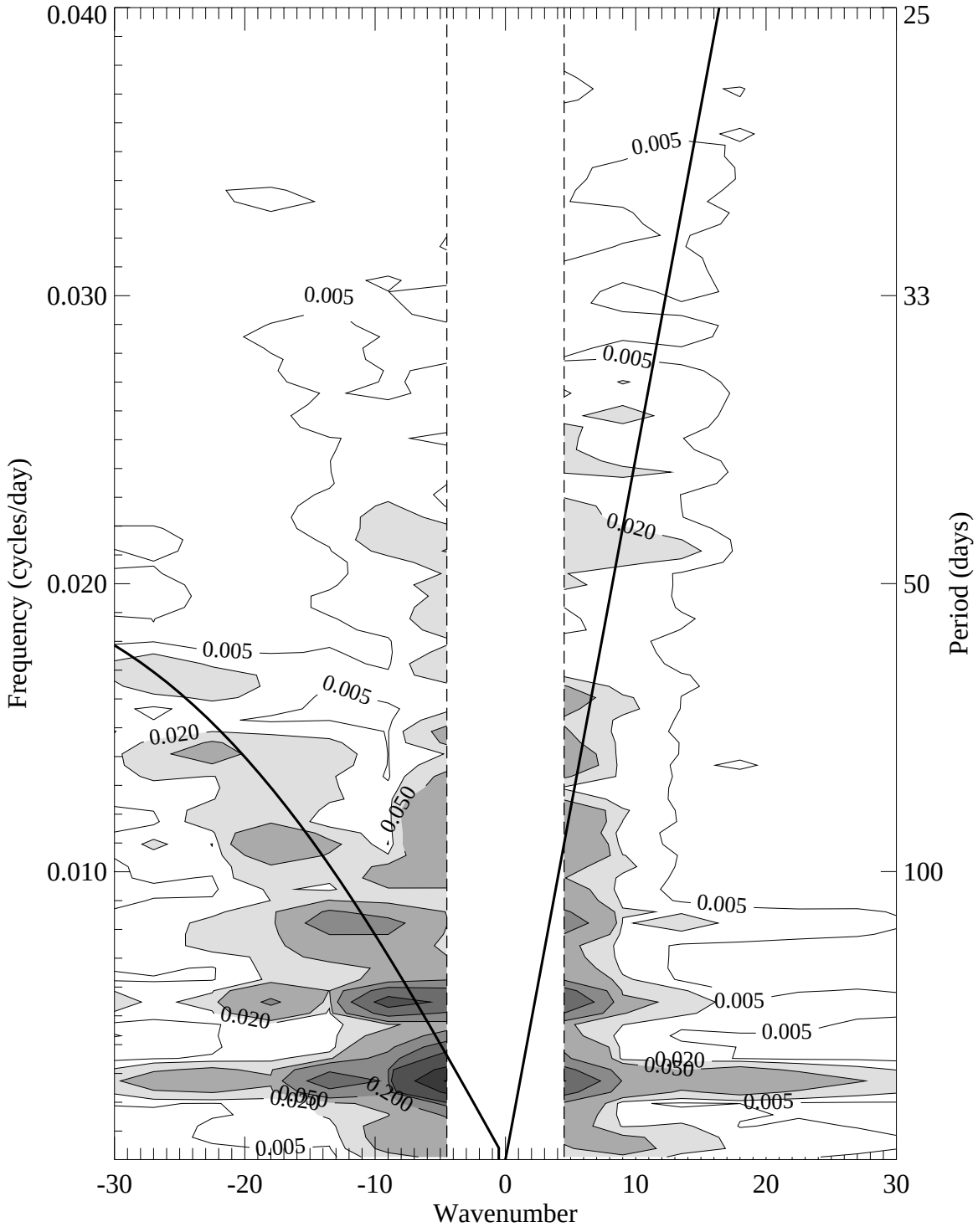

Figure 16: Wavenumber/frequency spectrum of model equatorial u_1. Axes as in Fig. 14. Contours in units of percent variance of $(ms^{-1})^2$. Vertical dashed lines correspond to planetary wavenumbers lower than 4.5, which cannot be resolved. The curved line on the left of the diagram corresponds to the dispersion curve for the equatorial $n = 1$ Rossby wave with an equivalent depth $H_e = 0.13m$. The line on the right corresponds to the dispersion curve for the equatorial $n = 1$ Kelvin wave with a similar equivalent depth (Gill 1982).

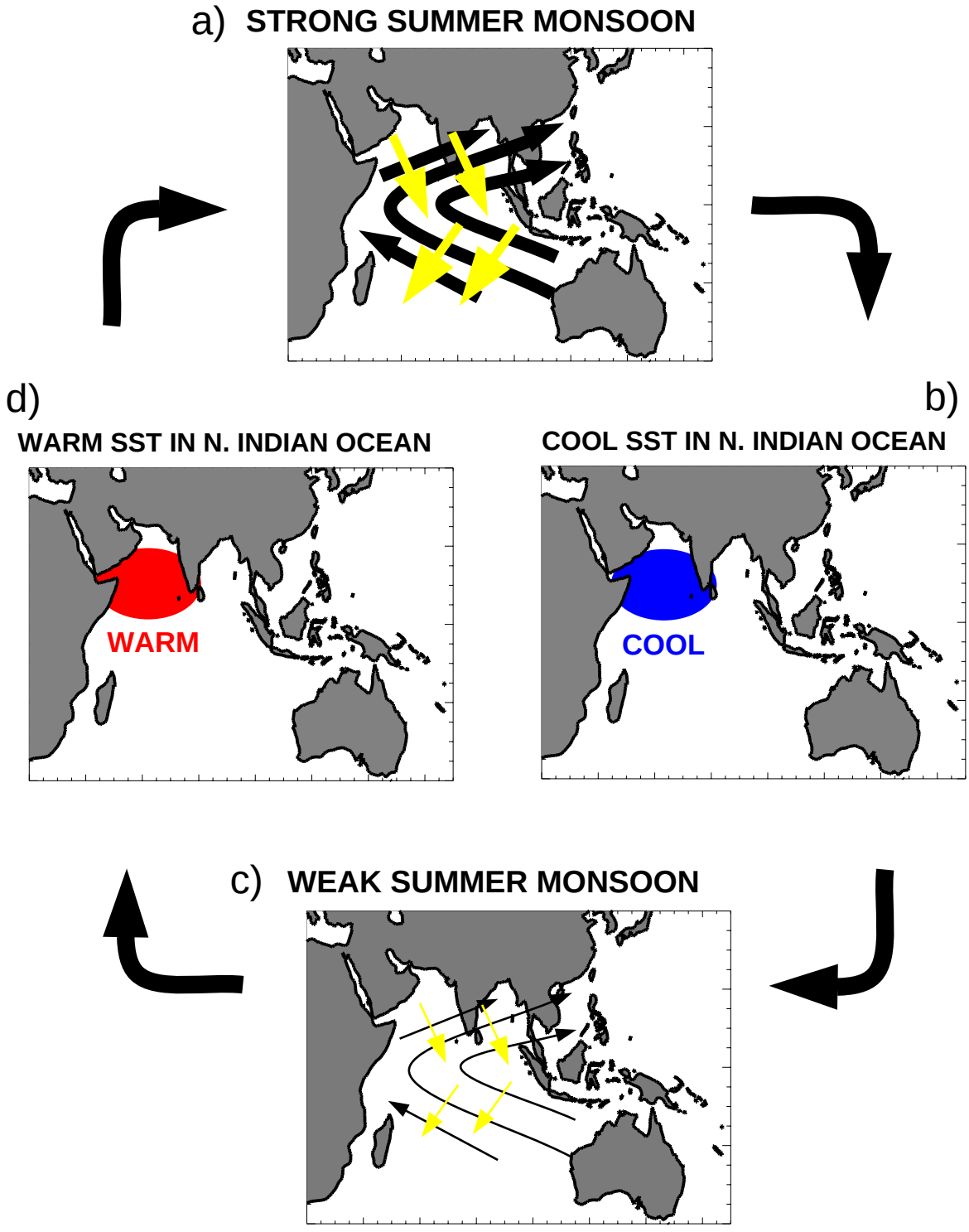

Figure 17: A possible biennial cycle of heat transport and SST anomalies for the northern Indian Ocean. The cycle arbitrarily starts at the uppermost panel (a), with a "strong" monsoon year. Curved black arrows denote the wind forced by the large-scale differential heating denoted by the warm (red) and cool (blue) hemispheres. The small yellow arrows are the Ekman transports forced by the winds, which are to the south on both sides of the equator. The resulting strong southward heat transports leave the northern Indian Ocean with cool SST anomalies (b), which contribute to the development of a "weak" monsoon the following boreal summer (c), depicted by weaker surface winds and weaker Ekman heat transports. The weak Ekman transports leave the northern Indian Ocean with warm SST anomalies (d), which contribute to a "strong" monsoon the following boreal summer (a).